

Recent Progress in Implantable Drug Delivery Systems

Guang-Qin He, Haimei Li, Junyi Liu, Yu-Lin Hu, Yi Liu,* Zhong Lin Wang,*
and Peng Jiang*

In recent years, tremendous effort is devoted to developing platforms, such as implantable drug delivery systems (IDDSs), with temporally and spatially controlled drug release capabilities and improved adherence. IDDSs have multiple advantages: i) the timing and location of drug delivery can be controlled by patients using specific stimuli (light, sound, electricity, magnetism, etc.). Some intelligent “closed-loop” IDDS can even realize self-management without human participation. ii) IDDSs enable continuous and stable delivery of drugs over a long period (months to years) and iii) to administer drugs directly to the lesion, thereby helping reduce dosage and side effects. iv) IDDSs enable personalized drug delivery according to patient needs. The high demand for such systems has prompted scientists to make efforts to develop intelligent IDDS. In this review, several common stimulus-responsive mechanisms including endogenous (e.g., pH, reactive oxygen species, proteins, etc.) and exogenous stimuli (e.g., light, sound, electricity, magnetism, etc.), are given in detail. Besides, several types of IDDS reported in recent years are reviewed, including various stimulus-responsive systems based on the above mechanisms, radio frequency-controlled IDDS, “closed-loop” IDDS, self-powered IDDS, etc. Finally, the advantages and disadvantages of various IDDS, bottleneck problems, and possible solutions are analyzed to provide directions for subsequent research.

Taking oral administration of non-steroidal anti-inflammatory drugs may damage the gastrointestinal tract. The acid-base environment of the gastrointestinal tract may also affect the release and absorption of active ingredients in drug carriers and even lead to inactivation of the active ingredients.^[2] Besides, repeated dosing is necessary to maintain adequate levels of drugs within the therapeutic window; this can increase the risk of drug resistance and side effects, as well as potential drug abuse. This effect is even more pronounced in people with chronic diseases. They may forget to take their medication or abandon the treatment directly. Blaschke et al. summarized drug use in 95 clinical studies. After 100 days of clinical trials, 20% had stopped taking the drugs; and year later, only 40% were still on treatment.^[3] In Europe, non-compliance with prescribed medications causes up to 20 0000 deaths and 125 billion euros in medical losses every year.^[4] These problems, if not alleviated, these problems will significantly increase the burden on healthcare systems. Therapeutic drug monitoring (TDM) is necessary for drugs with high toxicity and a narrow safety range.

Therefore, tremendous efforts have been devoted to developing a drug delivery platform with temporally and spatially controlled drug release capabilities. With the development of materials science, biomedicine, energy, and microelectronics technology, great progress has been made in the study of the controlled

1. Introduction

The efficacy of clinical, therapeutic treatments is highly dependent on the drug delivery method. Traditional drug delivery methods that rely on systemic administration, such as oral and intravenous, may have side effects and low bioavailability.^[1]

G.-Q. He, H. Li, Y.-L. Hu, P. Jiang
Department of Orthopedics Trauma and Microsurgery
Zhongnan Hospital of Wuhan University
School of Pharmaceutical Sciences
Wuhan University
Wuhan 430071, China
E-mail: jiangpeng@whu.edu.cn

G.-Q. He, H. Li, Y.-L. Hu, P. Jiang
Key Laboratory of Combinatorial Biosynthesis and Drug Discovery
Ministry of Education
Wuhan University
Wuhan 430071, China

J. Liu
Albany Medical College
New York 12208, USA

 The ORCID identification number(s) for the author(s) of this article can be found under <https://doi.org/10.1002/adma.202312530>

DOI: 10.1002/adma.202312530

Y. Liu
State Key Laboratory of Separation Membrane and Membrane Process & Tianjin Key Laboratory of Green Chemical Technology and Process Engineering
School of Chemistry and Chemical Engineering
Tiangong University
Tianjin 300387, China
E-mail: yiliu@whu.edu.cn

Z. L. Wang
Beijing Institute of Nanoenergy and Nanosystems
Chinese Academy of Sciences
Beijing 100083, China
E-mail: zhong.wang@mse.gatech.edu

P. Jiang
Hubei Jiangxia Laboratory
Wuhan 430200, China

release of drugs. Since 1950s, drug delivery systems (DDSs) have been divided into three generations. In 1952, Smith Kline & French introduced the first controlled-release formulation of dextroamphetamine to treat depression.^[5] Subsequently, this technique was used to develop oral and transdermal patches. That is, the first-generation DDSs did not have or had some simple controlled release capabilities, such as oral drugs, transdermal patches, and sustained-release agents, and need to be administered regularly and quantitatively by patients. The second-generation DDSs achieved a stimulus response and zero-order release. These stimulus-response systems can respond to physiological environments (enzymes, proteins, pH, etc.) or external physical signals (optical, acoustic, electrical, magnetic, etc.) to release drugs in a controllable manner. The second-generation controlled-release technologies, such as microneedles,^[6] iontophoresis,^[7] prodrugs,^[8] and gastroretentive systems,^[9] have multiple advantages. They circumvent first-pass effects, improve drug bioavailability, and protect active components from destruction by the digestive tract. However, they are not suitable for patients with chronic diseases who require long-term medication. Therefore, scientists are putting great effort into developing a new generation of DDSs. Currently, there is no specific classification of next-generation DDSs, but the main development tendency is to develop an intelligent controlled release system that integrates health monitoring, disease diagnosis, and drug delivery capabilities to achieve precision and personalized medicine. The IDDSs have many advantages that make them ideal for the treatment of chronic diseases: (i) response to signals in and out of the body, (ii) controllable timing and location of release, (iii) tailoring to the patient, and (iv) long working life. What is exciting is that the emergence of some closed-loop IDDSs offers hope that people suffering from chronic diseases can live normally rather than having to inject or take drugs for long periods of time.

An IDDS can be implanted into the body through minimally invasive surgery to achieve sustained and controllable drug release. The service life of an IDDS varies from several months to several years. For example, Liletta® 52-mg, an intrauterine device, can consistently release levonorgestrel for more than 6 years after intrauterine implantation.^[10] In 2022, a supplementary drug application was approved, extending the working life of the device to 8 years. An IDDS can be implanted in the disease focus directly or in other easily operated areas (e.g., subcutaneous implantation) and deliver drugs to the disease focus through a catheter.^[11] This technique avoids first-pass effects, improves bioavailability, and prevents damage to normal tissues. Moreover, the shape of the implant, drug formulation, and release mode can be customized for the patient to realize personalized medication. Over the past few decades, IDDSs have gained significant attention in the medical market because of their advantages. As of 2020, the global IDDS market size is \$21.8 billion and is expected to grow to \$31.6 billion by 2025.^[12]

IDDSs have been reported in a variety of forms, including hydrogels (such as alginate, methacrylate, chitosan, and glucan), thin films (such as poly (3,4-ethylenedioxythiophene) (PEDOT) and polypyrrole (PPy)), polymer fiber scaffolds, microreservoir arrays, and microelectromechanical systems. Some simple systems release drugs via free diffusion or erosion.^[13] Combined with 3D printing technology, these systems can achieve dual-

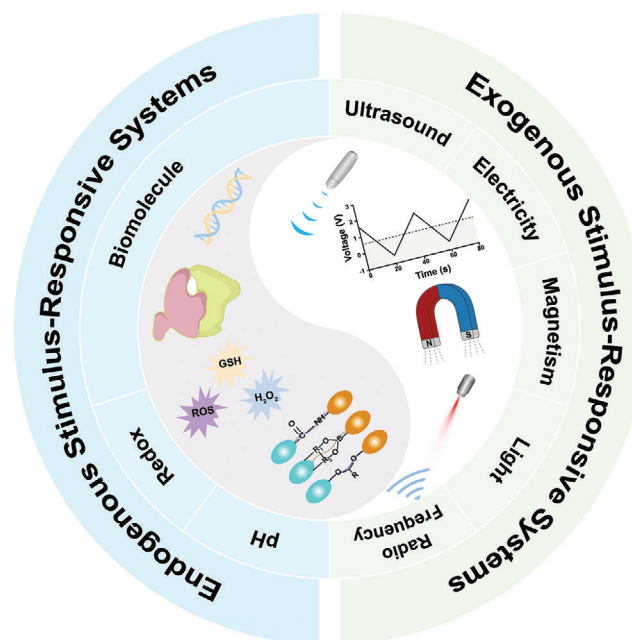


Figure 1. Overview of IDDS types alongside clinical and research applications presented in this review.

drug controlled release and inhibit tumor cell proliferation and metastasis through combined chemotherapy.^[14] The integration of stimulus-responsive materials (such as light-, heat-, and acid-sensitive materials) in the main structure can make these IDDSs respond to specific signal stimuli, such as changes in redox state and hydrophilic/hydrophobic balance, swelling/deswelling, and solid–liquid transition. After implantation, drugs are released by interaction with the microenvironment at the implant site or by receiving artificially applied signals from outside the body.

In this review, several types of IDDSs, including various stimulus-responsive systems (such as light, sound, electricity, magnetism, pH, and protein), radio frequency controlled IDDSs, “closed-loop” IDDSs, and self-powered IDDSs, reported in recent years are reviewed (Figure 1). Furthermore, the challenges related to technical and biological issues are discussed.

2. Endogenous Stimulus-Responsive IDDS

Diseased human tissues often have different physiological conditions from normal tissues. For example, the pH of the tumors is 5.0–6.5, compared to 7.4 in the normal tissues, and the concentration of GSH in tumor tissue was 4 times higher than that in normal tissue.^[15] In addition, the occurrence and progression of disease are often accompanied by abnormal expression of biomarkers such as proteins, enzymes, and cytokines. Therefore, triggering drug release in an abnormal physiological environment and disease biomarkers is an effective strategy for achieving specific controlled release.

2.1. Acid-Sensitive Drug Release

Acid-sensitive IDDSs usually contain acid-sensitive linkages (such as acetals, Schiff bases, and ortho esters) to conjugate

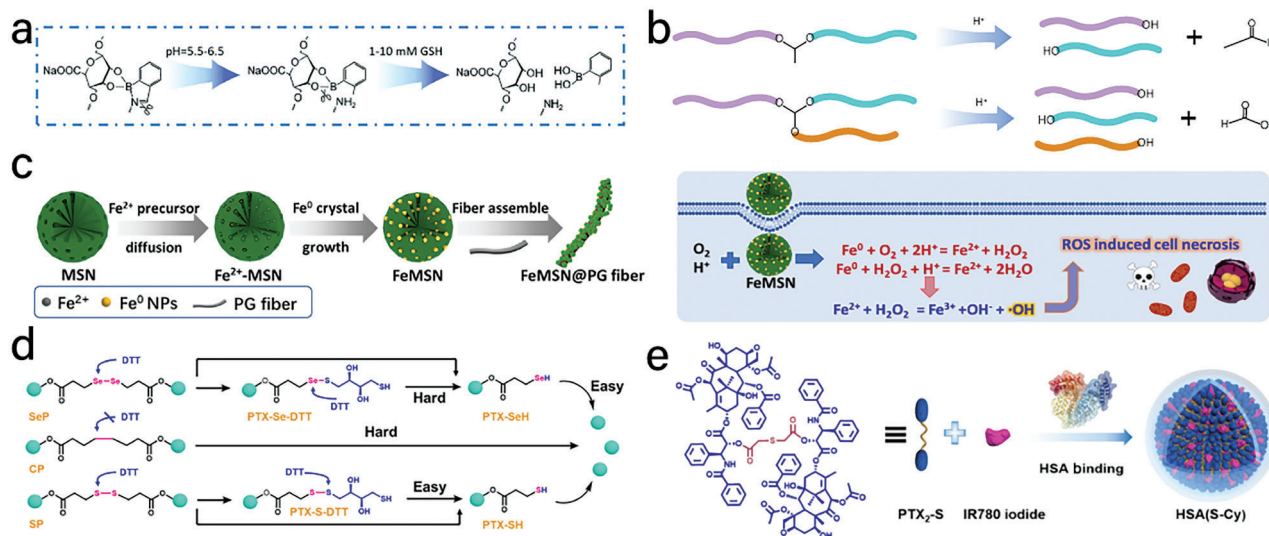


Figure 2. a) Redox/pH dual-responsive mechanism of drug carriers. Reproduced with permission.^[16] Copyright 2021, The Royal Society of Chemistry. b) Structure of pH-sensitive acetal and ortho ester. c) Schematic illustration of the synthesis of Fe⁰ nanocrystal embedded implantable chemotherapy platform FeMSN@PG fiber and its cell killing mechanism. Reproduced with permission.^[19] Copyright 2020, Elsevier. d) Reduction of disulfide and selenide bonds by dithiothreitol (DTT). Reproduced with permission.^[20] Copyright 2021, The American Chemical Society. e) Schematic diagram of albumin nanoparticles loaded with IR780 and paclitaxel dimer prodrug PTX₂-S containing thioether bonds. Reproduced with permission.^[21] Copyright 2019, Springer Link.

drugs and/or carriers (Figure 2a,b).^[16] Sarmah et al. developed a pH-sensitive hydrogel using dynamic Schiff-base bonds as pH-responsive linker to conjugate dialdehyde derivatives of starch and amino modified “chitosan.” Drug release in the hydrogel was controlled by pH, which exhibited the maximum release of ampicillin at a pH of 1.2, and the release decreased with increasing pH. Bacteriostatic experiments showed that the hydrogels loaded with ampicillin showed significant antibacterial activity against the tested bacterial strains.^[17] Lin et al. used diacetone-acrylamide, di(ethylene glycol) ethyl ether acrylate, and oligo(ethylene glycol) methyl ether acrylate as raw materials to synthesize an intermediate, which was then crosslinked with adipic acid dihydrazide to form a hydrogel through dynamic acylhydrazone covalent bonds. The hydrazone bonds were very sensitive to pH changes, and a small drop in pH (from 7.4 to 6.8) will cause a significant change in release profiles. Bovine serum albumin and glucose oxidase showed similar release in the hydrogels. At pH = 7.4, only ≈33% of glucose oxidase was released within 7 days. However, at pH = 6.0, the release reached 60% on day one.^[18] Acid-catalyzed reactions are another strategy used to trigger drug release. Wang et al. embedded Fe⁰ nanocrystals into the pores of mesoporous silica nanoparticles (FeMSNs) and designed an implantable chemotherapy platform (FeMSN@PG fiber) by combining FeMSNs with PCL-gelatin fibers (Figure 2c). After implantation at the tumor site, the FeMSNs were replaced by H⁺ and reacted with oxygen in the presence of H⁺ to produce H₂O₂, which was then converted into hydroxyl free radicals to kill cancer cells.^[19]

2.2. ROS-Sensitive Drug Release

Sensitive bonds in redox-responsive systems are mainly disulfide linkers, diselenide bonds, and thioethers (Figure 2d,e).^[20,22]

These chemical bonds are easily reduced or oxidized by the abnormal physiological environment in diseased tissues, such as high level of GSH and H₂O₂. The reactive oxygen species, including hydroxyl radical (·OH), superoxide (·O₂⁻), singlet oxygen (¹O₂) and hydrogen peroxide (H₂O₂), are highly oxidizing, and the abnormal expression of ROS is a hallmark of a variety of diseases. Therefore, ROS are effective factors in triggering specific drug delivery. Similar to pH-sensitive systems, ROS-sensitive systems connect drugs, carriers, or carrier monomers through redox-sensitive bonds. ROS-sensitive DDSs can be implanted directly into the lesion location to increase drug accumulation in the form of bulk materials such as hydrogels and polymer patches. Yao et al. integrated thioketal linkages into elastic polyurethane (PUTK) and electrospun them into fibrous polyurethane patches. Thioketal linkages can be decomposed by ROS, which are overexpressed in myocardial infarction, losing the PUTK structure and releasing the loaded glucocorticoid, methylprednisolone (MP). The PUTK/MP patch scavenged more than 60% of free radicals within 6 h, significantly promoted angiogenesis, and enhanced cardiac function after 28 days of treatment.^[23]

2.3. Biomolecule-Sensitive Drug Release

Diseases are often accompanied by cellular metabolic disorders and dysfunction, leading to abnormal physiological activities, such as the overexpression of enzymes and proteins. The use of abnormal physiological activity to trigger drug release is an effective approach. For example, Fu et al. encapsulated sunitinib nanodrugs in a hyaluronic acid-acrylate hydrogel to construct a matrix metalloproteinase-responsive hydrogel. Matrix metalloproteinases are highly expressed at tumor sites and can degrade the natural extracellular matrix and basement membrane to open up space for tumor proliferation. The hydrogel network was

Table 1. Advantages and disadvantages of different stimulus-responsive IDDSs.

Stimulus	Advantages	Disadvantages	References
Endogenous Stimulus (pH, ROS, Biomolecule, et al.)	Local delivery, sustained and active release	Cannot achieve “on-off” controlled release	[27]
Light	Spatiotemporal control, low cost, versatility (mediates PDT, PTT and imaging)	Phototoxicity, limited tissue penetration	[26]
Ultrasound	Spatiotemporal control, high tissue penetration and low cost, versatility (mediates SDT and imaging)	Not suitable for calcified and gas-containing tissues	[28, 29]
Magnetism	Spatiotemporal control, high tissue penetration, Imaging	Toxicity due to MNPs accumulation, susceptible to external magnetic field interference	[30]
Electricity	Spatiotemporal control, electronic equipment is highly integrated and miniaturized	Limitations of potential biosafety hazards and battery capacity	[31, 32]
Radio Frequency	Spatiotemporal control, data telemetry and power transfer	Distance-sensitive, complex structure	[33]

cross-linked by sensitive peptides that could be cleaved by matrix metalloproteinases, resulting in hydrogel collapse to release the sunitinib nanodrugs.^[24] Lu et al. combined calcium phosphate (CaP) nanosheets with vancomycin-loaded hydrogel microspheres using microfluidic technology to prepare a composite hydrogel for treating bone defects. Among them, vancomycin and hydrogels are covalently linked through oligonucleotide linkers, which can be specifically cut by the nuclease and Ca²⁺ of bacteria at the site of infection to release vancomycin, thus playing an antibacterial role. Simultaneously, calcium phosphate nanosheets were released from the gel pores to promote bone-defect repair.^[25]

3. Exogenous Stimulus-Responsive IDDS

Endogenous stimulus-responsive IDDS can accurately control drug release at the lesion sites. However, these technologies are not suitable for applications where the physiological environment does not change significantly, such as cancer prognosis and vaccination. In addition, endogenous stimulus often irreversibly disrupt the carrier material, making it impossible to achieve “on-off” controlled release (Table 1). In order to avoid abnormal drug concentrations at the implant site (too high or too low), it is necessary to carefully modulate the carrier material formulation and drug load.

Exogenous stimulus-responsive systems can respond to light, ultrasound, electricity, magnetism, and other signals, and release loads. These signals have little cross-reactivity with cellular signaling networks and little influence on biological tissues, which can improve the spatiotemporal precision of drug delivery with minimal side effects.^[26] In this context, exogenous stimulus-responsive drug delivery systems have been extensively developed and explored to achieve site-specific cargo release and activation by precisely controlling the site, intensity, and duration of the signal application.

3.1. Photo-Responsive IDDS

As an exogenous stimulus signal, light has unique advantages such as non-invasiveness, high spatiotemporal precision, and relatively low cost. As an electromagnetic wave, light can transfer its

energy to targets, causing a temperature increase, state change, and the breaking of chemical bonds. Therefore, light is a powerful tool for manipulating IDDS, and many photosensitive drug delivery systems have been developed to enhance delivery precision.

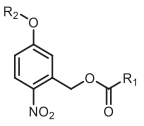
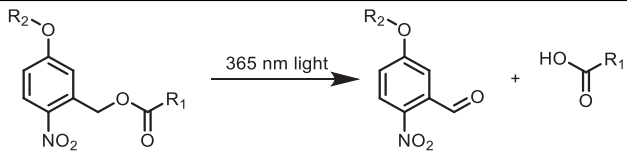
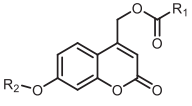
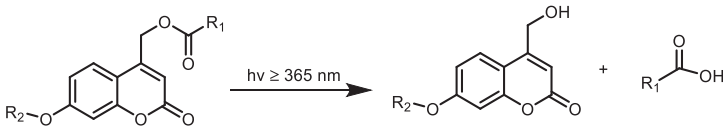
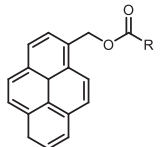
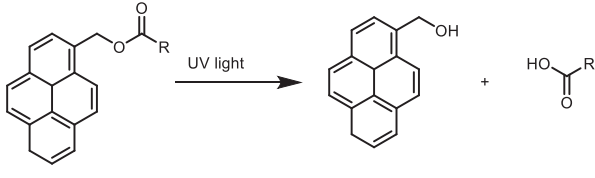
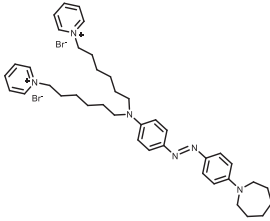
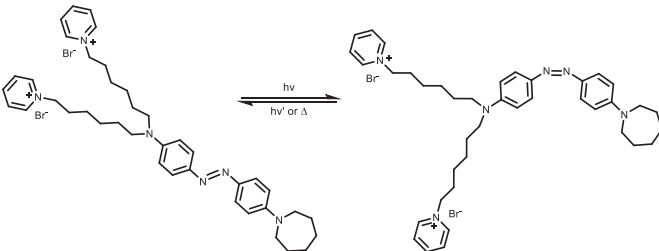
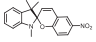
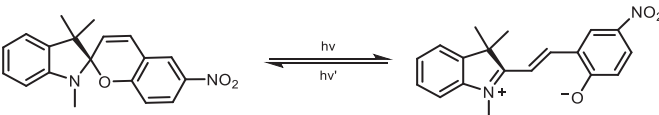
The choice of the wavelength is critical for photosensitive systems. Ultraviolet (UV) (100–400 nm) can provide high energy for bond cleavage but can also induce significant photo-damage to biomolecules and tissues. Some polymers and photosensitive small molecules can respond to visible light (400–750 nm), such as vitamin B12 derivatives, ruthenium complexes, and trithiocarbonate which are promising alternatives to UV-responsive systems.^[26] However, limited penetration depth remains a barrier to photo-responsive IDDS. Extending the photo-sensitive spectral range to the near-infrared (NIR I: 700–1000 nm, NIR II: 1000–1700 nm) window will expand the application of photo-responsive IDDS because light in the NIR window possesses stronger tissue penetration ability and lower photodamage than the ultraviolet-visible window.^[34]

According to the classification of response mechanisms, photosensitive IDDS can be divided into two categories: direct and indirect photo-responsive. Direct photo-responsive systems use light to directly trigger drug release, including photocleavage-triggered drug release, photoisomerization-triggered drug release, and photothermal-induced drug release.^[40] Indirect photo-responsive systems typically utilize light-induced intermediate reaction products such as ROS to trigger the release of loaded drugs. Such systems often carry photosensitizers as ROS sources and trigger load release through the cleavage of ROS-sensitive bonds.

3.1.1. Photocleavage Triggered Drug Release

Photocleavage refers to the irreversible rupture of carrier linkers under light irradiation. When the hydrophilic/hydrophobic balance is disrupted or the polymer chain is broken, the system collapses and releases the drug. These photosensitive structures including *o*-nitrobenzyl ester, coumarinyl, and pyrenyl-methyl esters (Table 2).^[41] Kharkar et al. designed a GSH-based photodegradable hydrogel. The *o*-nitrobenzyl arylthiol moiety in the hydrogel can be cleaved by UV light at 365 nm, and the

Table 2. Common light sensitive structures and their response mechanism.

Structures	Response mechanism
<p>O-nitrobenzyl ester^[35]</p> 	
<p>Coumarinyl ester^[36]</p> 	
<p>Pyrenylmethyl ester^[37]</p> 	
<p>Azobenzene^[38]</p> 	
<p>Spiropyran^[39]</p> 	

succinimide thioether linkages can undergo thiol exchange reactions with GSH, resulting in further breakage of the hydrogel crosslinks. The hydrogel was implanted subcutaneously into mice for controlled release of fibroblast growth factor-2.^[42] Wei et al. constructed functional hydrogels using polyethylene glycol (PEG) and a 5-methylfurfuryl grafted carboxymethyl chitosan derivative (CMCS-MF). The two ends of the synthesized photo-sensitive PEG derivatives are esters formed by maleic acid and *o*-nitrobenzyl. The maleacyl groups at both ends of the PEG derivatives were linked to 5-methylfurfural on CMCS-MF via a Diels-Alder (DA) reaction to form a photodegradable hydrogel (PNC gel). Under UV irradiation (365 nm), the active *o*-nitrobenzaldehyde produced by the photolysis of *o*-nitrobenzyl is cross-linked with an amino group through a Schiff base bond to form a pH-sensitive linker. The hydrogel was further cleaved under acidic conditions to achieve cascade degradation (Figure 3a). The dual-signal response system can control the load release more precisely than a single stimulus.^[43]

The penetration depth of ultraviolet light is a main limitation of photocleavage-triggered DDSs. An important solution is to use upconverting nanoparticles (UCNPs) to convert incident light at long wavelengths into shorter wavelengths

and higher energy light because NIR light has a larger penetration depth than UV and visible light. Yan et al. designed a hybrid polyacrylamide-poly(ethylene glycol) hydrogel, which was crosslinked by a photo-responsive *o*-nitrobenzyl group, and loaded core-shell NaYF₄:TmYb nanoparticles into the hydrogel. NaYF₄:TmYb nanoparticles act as up-conversion elements and emit ultraviolet light under 980 nm light irradiation to cleave the *o*-nitrobenzyl group, causing the hydrogel to change from a solid state to a liquid state, releasing encapsulated bovine serum albumin and trypsin.^[44] Bansal et al. designed a polyethylene glycol diacrylate hydrogel to co-encapsulate silica-coated NaYF₄:Yb³⁺/Tm³⁺ UCNPs and genetically modified cells. UCNPs convert NIR into blue light and activate genetically modified cells to express melanopsin (blue light reactive protein) and NFAT-shGLP-1 plasmid, which could mediate the in situ production of GLP-1 and promote the increase in insulin secretion in rat insulinoma cells (Figure 3b).^[45] Han et al. innovatively used the photoelectric effect of organic photovoltaics to power drug delivery systems. In this system, three organic photovoltaics coated with upconversion nanoparticles (NaYF₄:Yb and Er@NaYF₄:Nd, Yb) were connected in series and linked to a gold-film-encapsulated drug reservoir. Under NIR irradiation, UCNPs emit visible green

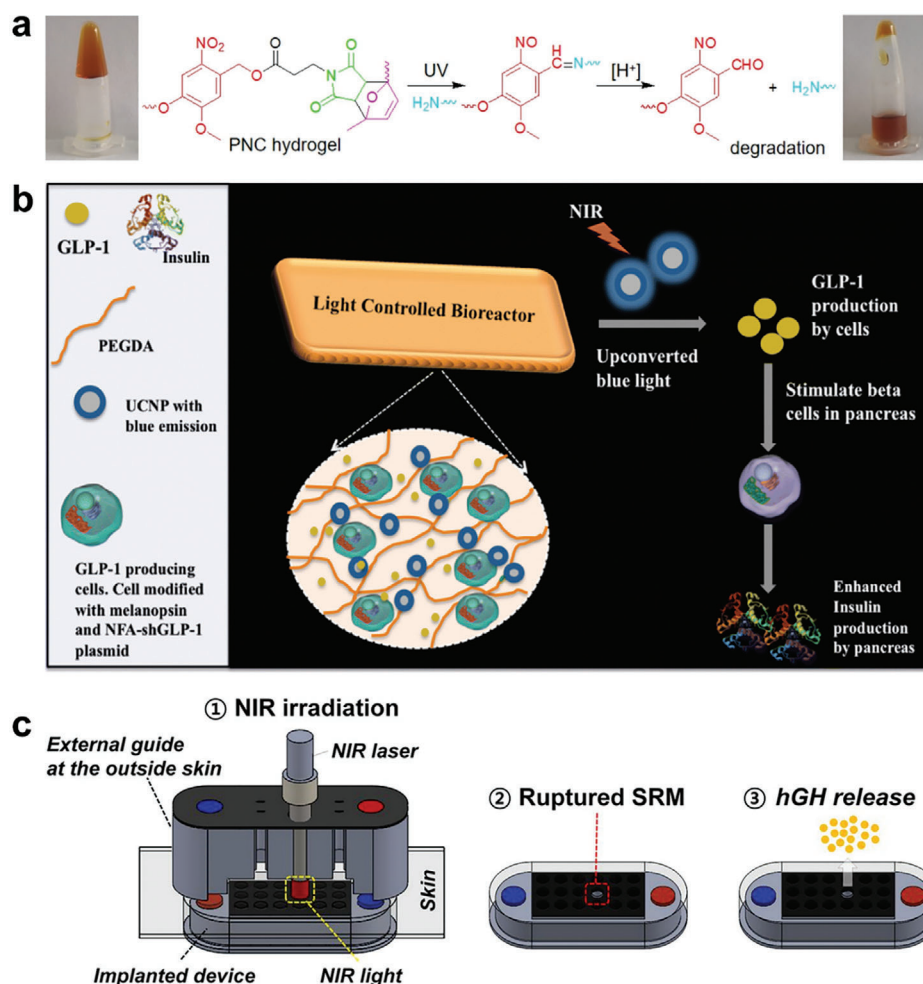


Figure 3. a) Photo-induced cascade degradation of PNC gel. Reproduced with permission.^[43] Copyright 2021, Elsevier. b) Schematic showing the use of UCNP for NIR-mediated GLP-1 production from optogenetically modified cells encapsulated in a light-guiding hydrogel. Reproduced with permission.^[45] Copyright 2023, Royal Society of Chemistry. c) Working principle of the polyurethane drug reservoir. Reproduced with permission.^[47] Copyright 2019, Proceedings of the National Academy of Sciences of the United States of America.

and red light, generating a voltage higher than 1.8 V through photoelectric conversion, causing dissolution of the gold film and release of the model drug (Rhodamine B).^[46]

3.1.2. Photoisomerization Triggered Drug Release

Photoisomerization is a process by which molecules undergo reversible structural transformations under light irradiation. These processes mainly include *cis*-/*trans*- structural transitions (azobenzene, stilbene, etc.) and open-loop/closed-loop transitions (spiropyran, retinoyl, 2-diazo-1,2-naphthoquinone, etc.) (Table 2).^[48] The change in structure is accompanied by changes in polarity and solubility, which causes the system to collapse and release the load. Taking azobenzene as an example, the two benzene rings of azobenzene are connected by N = N. Azobenzene in *trans* structure can exist stably owing to the small steric hindrance and close arrangement. *Trans*-azobenzene transforms into *cis* structure after absorbing 320–350 nm photons, and when exposed to 400–450 nm visible light, a configuration flip oc-

curs to restore *trans* structure.^[49] Controlled drug release can be achieved using azobenzene as a linker to design prodrug or transport vehicle.^[50] Muller-Deku et al. attached azobenzene to paclitaxel 3'-amine and designed a panel of 3-azobenzamide-taxanes (AzTax) for biological testing. The half-life of Z-AzTax can be adjusted from 24 h to 50 days by changing the substituents on the distal ring of azobenzene.^[51] This research enables the on-demand regulation of the microtubule cytoskeleton to prevent the disruption of relevant biological reactions. However, azobenzene further reduces the water solubility of paclitaxel, and additional technology is required to solve this problem. Liposomes have multiple advantages in drug delivery, such as good dispersion in aqueous solutions, which can improve the dispersion and stability of lipophilic drugs, and similar components to the cell membrane can promote cell internalization. Chander et al. synthesized photosensitive phosphatidylcholine analogs by adding azobenzene to the lipid tail, inserting it into liposome membranes, and encapsulating DOX (PaLNPs). Under UV irradiation (365 nm), *trans*-azobenzene changes to a *cis*-structure, triggering DOX release and exhibiting cytotoxicity similar to that

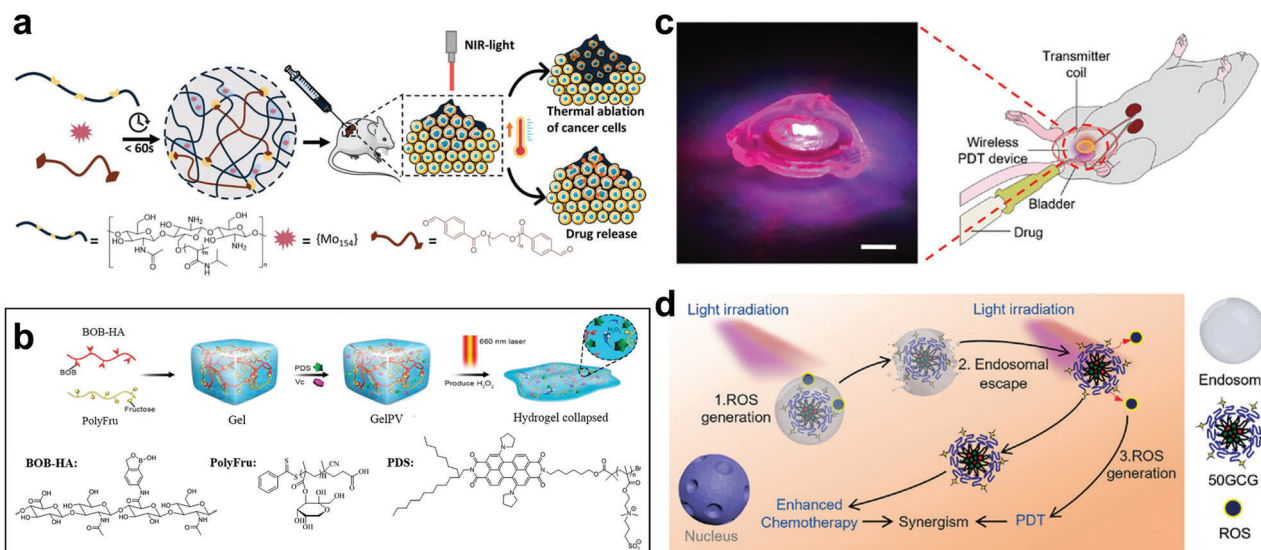


Figure 4. a) General scheme showing the design, preparation, and synergistic effects of PTT and NIR-triggered DOX release from Mo_{154} Gel. Reproduced with permission.^[56] Copyright 2021, Wiley. b) Schematic diagram of molecular structures and NIR light-induced degradation of GelPV. Reproduced with permission.^[58] Copyright 2020, The American Chemical Society. c) Photograph of the micro-LED and the schematic of treatment strategy in mice orthotopic bladder cancer model. d) Schematic illustration of the mechanism of Ce6 and GemE co-loaded glycosylated carrier for a synergistic combination of PDT and chemotherapy because of PCI effect. Reproduced with permission.^[59] Copyright 2023, Wiley.

of free DOX. Considering the limited tissue penetration depth of light, the authors designed red-shifted azobenzene liposomes (red-PalNPs) in which -Cl was added to the N = N *ortho*-position of the azobenzene ring to redshift the absorption wavelength to 660 nm.^[52]

3.1.3. Photothermal Triggered Drug Release

There are three main types of photothermal conversion principles: (I) surface plasmon resonance (SPR); (II) band gap transition; (III) π - π^* transition. The most common photothermal agents include small molecules (such as indocyanine green and pullulan), carbon materials (such as graphene and carbon nanotubes), metal nanoparticles (Au, Ag, Pt, etc.), metal oxides and sulfides (Ag_2S , CuS , MoS_2 , MnO_2 , Fe_3O_4 , etc.), metal-organic skeletons, and photosensitive polymers (such as polydopamine). Photothermal heating locally elevates the temperature, causing changes in the porosity and physical state of the carrier, and resulting in cargo release.^[53] Chen et al. prepared NIR-responsive hydrogels by evenly dispersing cellulose nanocrystals (CNCs) and Fe_3O_4 nanoparticles ($\text{Fe}_3\text{O}_4/\text{CNCs}$) in poly(*N*-isopropylacrylamide) (PNIPAm) networks. After irradiation with 808 nm light for 80 s, the temperature of the PNIPAm gel increased from room temperature to 41 °C, and the release of vancomycin reached 47% within 2 h. During the 80 h study period, the amount of vancomycin released by the NIR irradiation group was 1.4 times that of the control group.^[54] Lee et al. reported a polyurethane drug storage system consisting of 18 small drug-carrying tanks sealed with stimulus-responsive membranes (SRM). The SRM contained a thermosensitive polymer and reduced graphene oxide. A DDS implanted *in vivo* can respond to NIR light and release loaded human growth hormone (hGH) (Figure 3c). After 480 min of NIR irradiation, plasma insulin-

like growth factor concentration was $270.5 \pm 36.8 \text{ ng mL}^{-1}$, which was similar to that of intravenous injection group ($261.1 \pm 46.7 \text{ ng mL}^{-1}$).^[47] Liu et al. designed a gel-fiber scaffold that could be loaded with both hydrophilic and hydrophobic drugs. The scaffold was composed of alginate hydrogel, PCL, and PDA layers. The alginate layer can encapsulate hydrophilic drugs, the PCL layer can encapsulate hydrophobic drugs, and the PDA layer can mediate photothermal conversion to cause sol-gel transformation for drug release.^[55] Guedes et al. developed a self-healing hydrogel loaded with $\{\text{Mo}_{154}\}$ and DOX for synergistic photothermal and chemotherapy. The hydrogel formed a dynamic network through imine bond crosslinking between dibenzaldehyde-functionalized polyethylene glycol and poly(*N*-isopropylacrylamide)-functionalized chitosan (CS-g-PNIPAAm). The electrostatic interactions between anion $\{\text{Mo}_{154}\}$ and cationic CS-g-PNIPAAm further strengthened the gel network (Figure 4a). After hydrogel implantation, the local temperature can rise up to 50 °C under 808 nm light irradiation and the hydrogel completely degraded after two weeks.^[56]

3.1.4. ROS-Mediated Photo-Responsive Drug Release

ROS-mediated photo-responsive drug release systems often carry photosensitizers that produce ROS under light irradiation, triggering drug release by the cleavage of ROS-sensitive bonds. Photosensitizers include chlorin e6 (Ce6), pyropheophorbide a, and porphyrin.^[53a,57] Sun et al. designed a photodegradation hydrogel by encapsulating photosensitizer (perylene diimide zwitterionic polymer, PDS), ascorbic acid, DOX and photothermal nanoparticles. In mice, photosensitizers and ascorbic acid produced hydrogen peroxide under NIR irradiation, cleaving the dynamic covalent bonds of the hydrogel and releasing photothermal nanoparticles and DOX (Figure 4b).^[58] As mentioned above,

light penetration depth is a major challenge for photo-responsive IDDS. This problem can be addressed by using implantable LEDs. Sun et al. implanted a micro-LED that emitted purple (405 nm) and red (660 nm) light near the bladder to treat bladder cancer, in combination with nanodrugs loaded with photosensitizers and gemcitabine (GemE) (Figure 4c,d). The micro-LED device was 8 mm in diameter and 2 mm in thickness and could still operate 33 days after implantation.^[59] This strategy of local irradiation with a built-in light source not only breaks through the limit of light penetration depth, but also reduces phototoxicity.

3.2. Ultrasound-Responsive IDDS

Ultrasound is a safe, non-invasive signal that can penetrate tissues without causing damage. Hydrogels are commonly used in ultrasound-responsive implants. Ultrasound triggers the release of drugs from hydrogels, mainly through mechanical and thermal effects. The main driving forces that trigger drug release are the shear force and local high temperature generated by ultrasonic waves.^[60] Mechanical effects cause defects in the hydrogel, and the destruction is irreversible, making it impossible to achieve on-off control of drug release. Self-healing hydrogels can recover to their original state after ultrasound treatment and terminate drug release. In addition, the incorporation of nanoparticles to separate the ultrasonic response element from the hydrogel is a strategy for avoiding irreversible damage. By controlling ultrasonic energy, frequency, exposure time, and other parameters, the release rate can be controlled to achieve on-demand drug delivery.

3.2.1. Sono-Thermal Triggered Drug Release

The absorption of ultrasonic energy by biological tissues produces local hyperthermia, which can be directly used for tumor ablation. However, it is more common to associate the thermal effect with heat-sensitive materials, such as heat-sensitive liposomes, heat-sensitive hydrogels, and perfluorocarbons. For example, thermosensitive liposomes can be obtained by inserting a lysolipid component (such as 1-stearoyl-2-hydroxy-sn-glycero-3-phosphatidylcholine) into the phospholipid bilayer. Upon heating to the lipid transition temperature (typically 42–43 °C), pores appear on the bilayer leading to cargo release.^[61] Thermally sensitive hydrogels can undergo sol-gel transitions or structural changes under the sono-thermal effect to release the load. Huang et al. designed a hydrogel nanoparticle with a H₂S gas core for the treatment of pancreatic tumors. The nanoparticle shell was composed of gemcitabine coated with N-isopropylacrylamide, which is a thermosensitive polymer. The H₂S gas core oscillates under ultrasound to produce heat, resulting in shell contraction and drug release.^[62] Adding metal nanoparticles to hydrogel particles can increase acoustic impedance and enhance ultrasonic sensitivity. For example, Kubota et al. added tungsten particles to calcium alginate gel beads, which enhanced their ultrasonic sensitivity of gel particles and the ultrasonic-induced cargo release.^[63] Moreover, the addition of microbubbles or metal/metal oxide nanoparticles can also enhance the ultrasonic scattering effect of the gel and enhance the imaging contrast.^[64]

3.2.2. Sono-Mechanical Triggered Drug Release

In biological tissues, ultrasonic energy causes the microbubbles to oscillate. This creates a microstream around the bubble, which acts as a microinjector and facilitates drug infusion. Bubble collapse also produces high pressure and shear forces on nearby biofilms, changing their permeability and increasing the uptake of foreign molecules. Moreover, high pressure and shear force can also break the physical crosslinking or dynamic chemical bonds of the hydrogels (such as dynamic boronate ester bonds), collapsing the hydrogel or changing its pore size. Meng et al. prepared nanovaccines using ovalbumin (OVA) and imiquimote (R837) encapsulated in self-healing hydrogels (Figure 5a). When implanted into mice and exposed to ultrasound, these hydrogels collapsed, releasing ovalbumin.^[65] The porous nature of hydrogels often leads to undesired drug leakage. Sun et al. connected tannic acid to the hydrogel backbone via dynamic covalent boronate ester linkages to solve the leakage problem while also endowing the hydrogel with ultrasonic responsiveness. In addition, methacrylic hyaluronic acid and four-armed polyethylene glycol acrylate were used to construct a permanently crosslinked hydrogel network through free radical polymerization, which could enhance the mechanical stability of the hydrogel network.^[66]

3.2.3. Other Mechanism of Sono-Responsive Drug Release

Ultrasound-triggered in situ drug synthesis is another mechanism of sono-responsive drug release. Campbell et al. designed a miniature device consisting of an ultrasonic receiver, a rectifier, a UV LED, and interdigitated Pt electrodes. After implantation at the tumor site and driven by sonication outside the body, the device generated a current to cause the electrolysis of water and platinum electrodes, and lit a UV LED to synthesize cisplatin in situ (Figure 5b).^[67] Zhu et al. designed heat-sensitive hydrogel-enveloped piezoelectric tetragonal BaTiO₃ (T-BTO). The electrons and holes of tetragonal BaTiO₃ are unpaired under ultrasonic vibration and separated by piezoelectricity, creating a strong built-in electric field that catalyzes the generation of ROS such as toxic hydroxyl (•OH) and superoxide (•O²⁻) radicals in situ and eradicating tumors (Figure 5c). The gel caused significant apoptosis under ultrasound irradiation after implantation at the tumor site. The tumors of the ultrasound-treated mice were completely eradicated within five days and the mice survived for more than 40 days, whereas the control group survived for no more than a month (Figure 5d,e).^[68]

3.3. Magnetic-Responsive IDDS

In the field of biomedicine, the biggest advantage of magnetically responsive IDDS is the magnetic inertia of biological tissues, which does not cause tissue damage, and is not limited by penetration depth and phototoxicity. The interaction of the magnetic field with biological tissue is too insignificant to cause damage to the biological barrier. In addition, studies have shown that, when cells internalize magnetic nanoparticles (MNPs), external magnetic fields can temporarily destroy endothelial adhesion connec-

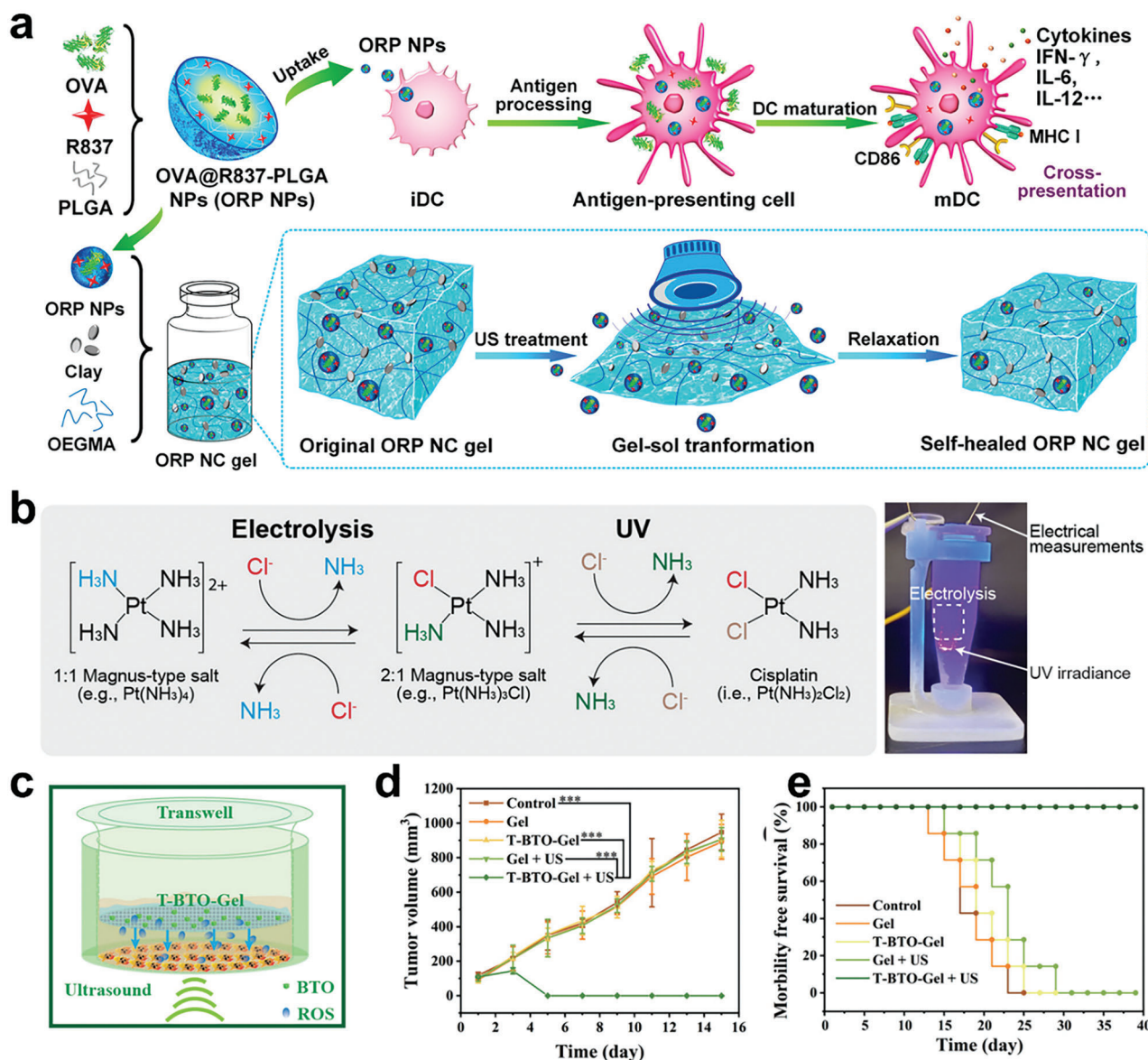


Figure 5. a) The scheme showing the fabrication of ORP NPs for immune stimulation as a nanovaccine and US-triggered release of ORP NPs from the NC gel. Reproduced with permission.^[65] Copyright 2021, The American Chemical Society. b) Scheme of the complete sequence of reactions and species involved in the microdevice's cisplatin synthesis and a picture of simultaneous electro- and photo-chemical reaction. Reproduced with permission.^[67] Copyright 2021, Wiley. c) Schematic illustration of cellular level piezocatalytic therapy in vitro. d) Time-dependent tumor-growth curves of tumor-bearing mice after different treatments. e) Survival curves of tumor-bearing mice after treatments. Reproduced with permission.^[68] Copyright 2020, Wiley.

tions, activate the bypass transport pathway of vascular endothelial cells, increase vascular endothelial permeability, and facilitate drug entry into tissues.^[69]

MNPs play an important role in magnetic triggering because they have strong magnetic moments that can respond sensitively to changes in an external magnetic field. Magnetic triggering depends on the response of magnetic components to external magnetic fields. There are two triggering mechanisms: the magnetothermal effect and magnetic deformation. In general, high-frequency alternating magnetic fields (AMFs) cause the thermal deposition of MNPs, resulting in changes in the heat-sensitive composition and triggering the release of cargoes. The static

magnetic field and low-frequency AMF can flip the magnetic moment of the MNPs, resulting in the disturbance of the MNPs, which leads to the deformation of the carrier and release of the cargo.^[30]

3.3.1. Magnetothermal Triggered Drug Release

The mechanism underlying the magnetothermal effect is complex. It is not only related to the properties of the nanoparticles themselves (such as size and microstructure), but also to the frequency and strength of the magnetic field, which includes the

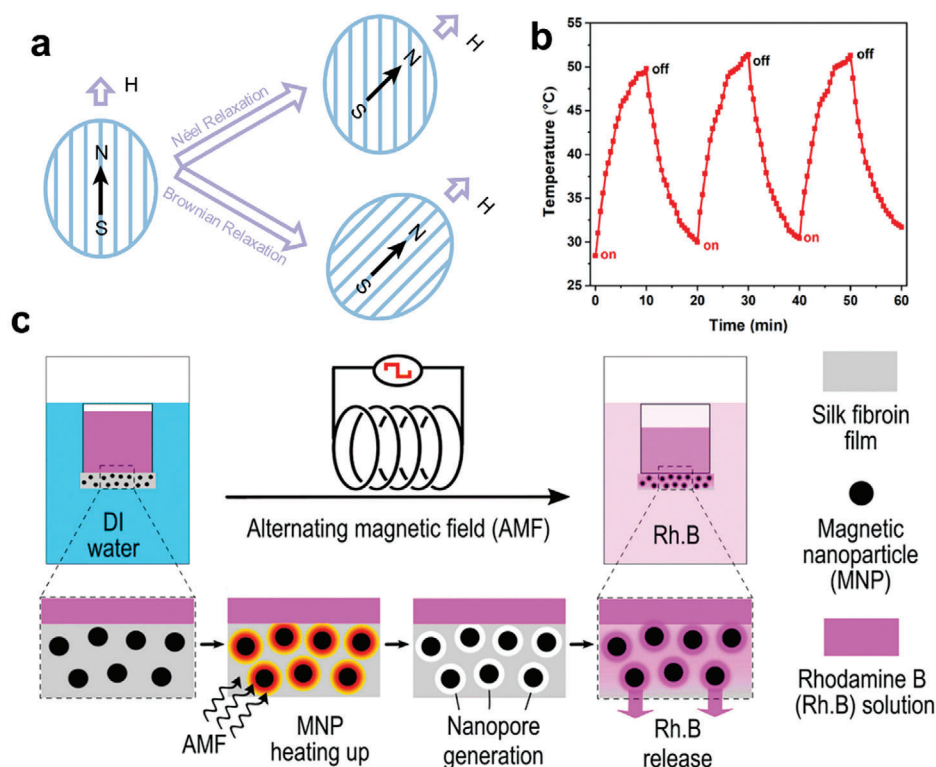


Figure 6. a) Mechanism of Néel relaxation and Brownian relaxation. b) In vitro heating curves of HA-DOPA-MNPs (2.0 wt.%, 4 mg mL⁻¹) hydrogel in three cycles of consecutive AMF irradiation. Reproduced with permission.^[72] Copyright 2021, Elsevier. (c) Silk/magnetic nanoparticles (silk/MNPs) composite membrane for controllable drug delivery with rhodamine (Rh.B) fluorescent dye as the model drug. Reproduced with permission.^[73] Copyright 2021, The American Chemical Society.

effect of magnetic strands, domain wall resonance, Néel relaxation, and other mechanisms. For superparamagnetic nanoparticles, the heat generation mechanisms are primarily Néel and Brownian relaxations. When the size of the superparamagnetic material was less than the critical value, the thermal motion of the nanoparticles quickly flipped and randomly oriented their magnetic moments. The vector sum of the magnetic moments is zero, and does not exhibit magnetism at the macro level. When an external magnetic field was applied, the magnetic moments of the nanoparticles aligned in the direction of the magnetic field. The magnetic moment changes in two ways: first, the nanoparticles do not move, the magnetic moment rotates, and the resulting electromagnetic loss is converted into heat energy, which is known as Néel relaxation. Second, the magnetic moment itself does not rotate, and the rotation of the nanoparticles causes the magnetic moment to align in the direction of the magnetic field. The interaction between the nanoparticles and the friction between the nanoparticles and the surrounding medium generates heat energy, which is called Brownian relaxation (Figure 6a).

The magnetothermal effect of MNPs can act directly on biological tissues and produce corresponding biological effects, such as thermal ablation of tumors and improvement of tumor hypoxia, which can be used as an auxiliary means for other therapeutic strategies.^[70] In DDS applications, the magnetothermal effect can be applied to temperature-sensitive drug delivery. A typical strategy involves the contraction or expansion of carrier

materials caused by the magnetothermal effect to trigger drug release. The most commonly used in this regard are superparamagnetic iron oxide nanoparticles (SPIONs), which have been approved by the FDA for the treatment of iron deficiency anemia in adults and as MRI contrast agents (e.g., Feraheme®).^[71]

Phase transition is another strategy used for temperature-sensitive DDS. Hydrogels are common phase-transition systems. Dai et al. used SPIONs as the crosslinking agent for dopamine and hyaluronic acid coupling gels, and the SPIONs formed coordination bonds with the catechol of dopamine to enhance the mechanical strength of the gel. Under AMF, the magnetothermal effect caused the gel temperature to rise, resulting in a sol-gel transition and the release of adriamycin.^[72] In each stimulation cycle, the temperature was increased from room temperature to 50 °C for 10 min of AMF stimulation, and then dropped back to 30 °C when the AMF was turned off (Figure 6b). The addition of SPIONs enhanced gel stability, thereby prolonging the retention time of DOX in vivo. Recently, Wang et al. proposed a new controlled-release strategy using the magnetothermal effect to induce thermal degradation of the drug reservoir encapsulation material and trigger drug release. A fully biodegradable composite membrane was fabricated using silk fibroin proteins and MNPs. The magnetothermal effect of MNPs in AMF causes thermal degradation of the fibroin protein and the formation of nanopores to release the drug solution (Figure 6c). The drug release rate can be controlled by varying the duration of AMF exposure.^[73]

3.3.2. Magnetic Deformation Triggered Drug Release

Under a low-frequency AMF or static magnetic field, the rotation of MNPs does not generate heat but can change the internal structure of the carrier. Gupta et al. deposited magnetite in situ in poly[2-(hydroxyethyl) ethyl methacrylate] to prepare superparamagnetic carriers for cisplatin delivery. In the presence of a magnetic field, the magnetic moments of the SPIONs tend to align in the direction of the external magnetic field, causing the SPIONs to rotate. This process led to relaxation of the polymer chain and enhanced cisplatin release.^[74] Aggregation of MNPs in a magnetic field typically causes the polymer to shrink, thereby blocking cargo release. Lin et al. synthesized magnetic β -cyclodextrin (β -CD)/cellulose hydrogel microspheres for delivery of 5-fluorouracil (5-FU). The external magnetic field caused the Fe_3O_4 NPs to aggregate, causing the gel to become compact, preventing the release of 5-FU. After removing the magnetic field, the Fe_3O_4 NPs dispersed, which enlarged the gel aperture and released 5-FU.^[75]

3.3.3. Other Magnetism-Responsive Mechanisms

More recently, Qian et al. designed a two-layer intrinsically magnetic epicardial patch (MagPatch), in which MNPs are not used directly to deliver drugs, but as magnetic markers for the location of drugs in magnetic fields. The bottom three layers of the patch were composed of poly (glycerol sebacate) and NdFeB (permanent magnet) to provide a magnetic field. The top was composed of poly (glycerol sebacate) and poly (ϵ -caprolactone), which acted as a magnetic shield. The endothelial cells internalized with SPION were inoculated on the patch surface, and the attraction between the magnetic field and SPION firmly attached the endothelial cells to the patch surface. After the patch was implanted into the myocardial infarction area of the mouse heart, the capillary density in the tissue recovered rapidly and built a network between heart and the patch (**Figure 7a**). After 28 days, the number of α -SMA (vascular smooth muscle cell marker) and CD31 (endothelial cell marker) positive vascular structures in tissues was significantly higher than that in other groups, indicating that the patch significantly promoted vascular regeneration. After 42 days, the magnetic properties of the patch were still similar to those of the initial implant. In addition, after intravenous injection of SPION-labeled nanovesicles, significant vesicle aggregation was observed at the heart site at a higher concentration than unlabeled nanovesicles, thanks to the capture of SPION by the magnetic patch.^[76]

Another type of magnetically-actuated system does not rely on SPION, but uses macro-scale magnets to control the drug reservoir through the principle of “same poles repel, different poles attract.” Lee et al. designed a microinjector that could accurately absorb the prescribed dose of liquid medicine and inject it into the lesion site under the control of external magnets. As shown in **Figure 7b**, when an external magnet was applied, the plunger was drawn upward, and the liquid in the loading tank was sucked into the cartridge. Conversely, when the magnet is removed, the plunger falls, injecting liquid from the cartridge into the biological tissue. The volume of liquid per injection could be controlled by increasing or decreasing the number

of outlet ports on the cartridge walls. The microinjector can function in the body for at least 30 days with a mild foreign body response and inflammation.^[77] The plunger could be patterned such that only a certain shaped magnet could pull the plunger, preventing interference from other magnetic fields.^[81] Iacovacci et al. designed a temporary drug reservoir (PILLSID), that could be implanted into the peritoneum and repeatedly refilled through the digestive tract. After the capsule was taken orally, the capsule traveled through the digestive tract to the implant device, and by magnetic docking, PILLSID popped up a small needle to transfer the drug from the capsule into the PILLSID. The PILLSID quantitatively injects drugs into the abdominal cavity through a catheter, and the capsules are naturally excreted through the digestive tract (**Figure 7c**).^[78] More recently, Zheng et al. recently developed an implantable magnetically actuated capsule (IMAC) for on-demand drug delivery. The capsule consists of two magnetic spheres, an elastic membrane, and a drug reservoir. Driven by a portable magnetic actuator (MA), the two magnetic balls repelled and moved away from each other, squeezing the elastic film and creating pressure to squeeze the liquid out of the drug reservoir (**Figure 7d**). Over the course of 15 days of in vivo administration, the capsule-treated diabetic rats showed pharmacokinetic and pharmacodynamic profiles that were highly similar to those of rats treated with subcutaneous injection, suggesting that the magnetically actuated capsule has powerful on-demand drug release properties.^[79]

3.4. Radio Frequency Field Controlled IDDS

Radio frequency (RF) is a high-frequency alternating electromagnetic wave that can pass through biological tissues noninvasively and cause a temperature increase by accelerating the relative motion between molecules. This effect was used to trigger release in the implanted device. Lee et al. developed a radio-frequency field-controlled IDDS consisting of an oxidized starch patch (OST) for DOX loading, an ultrathin magnesium electronic device for heating, and a wireless temperature sensor for controlling the heating (**Figure 7e**). After intracranial implantation in mice, the temperature of the IDDS was wirelessly controlled by an external alternating radio frequency field to trigger DOX release and increase the penetration depth of DOX into the brain tissue. Intracranial implantation allows drugs to cross the blood-brain barrier directly and increases drug accumulation at lesion sites.^[80] In implantable medical devices, radio frequency can be used to power the device or send commands to control device operation. Joo et al. designed a soft implantable drug delivery device that could be connected wirelessly to a wearable device and triggered subcutaneous drug release via wireless voltage induction for the emergency treatment of fatal epilepsy. The system consists of three components: an implantable drug reservoir, a transmitter, and an electrophysiological sensor. The drug transmitter was implanted in the subcutaneous area of the wrist and a watch-like power transmitter was worn above the implant site for wireless communication. An electrophysiological sensor was worn on the patient's head to monitor the physiological status. When a patient has a fatal seizure, the sensor detects an abnormal signal and sends a command to the transmitter to wirelessly

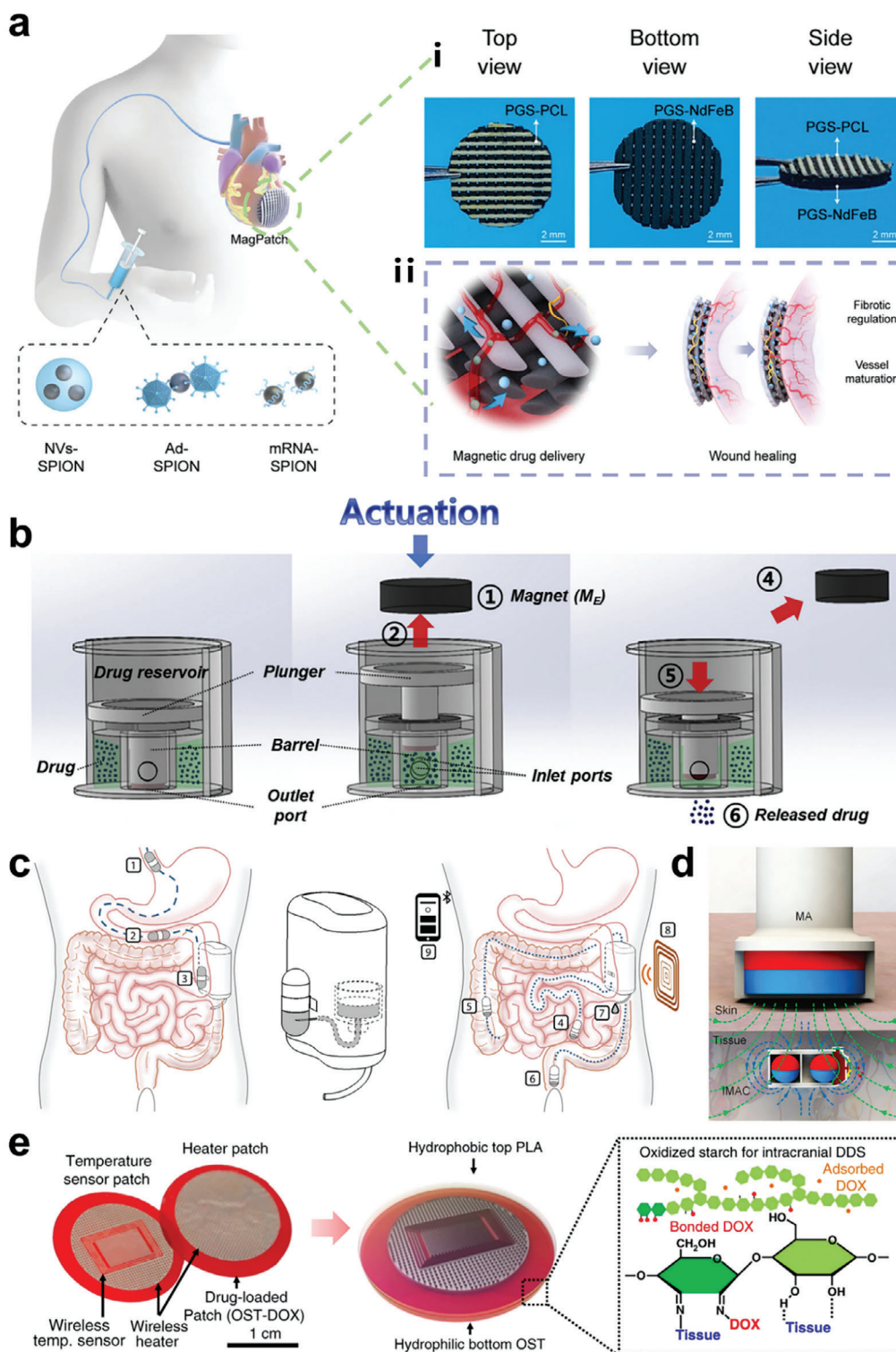


Figure 7. a) Schematic of the MagPatch therapy. i) Representative photographs of MagPatch. ii) MagPatch locates SPION labeled drugs at the implant site and promotes tissue repair. Reproduced with permission.^[76] Copyright 2023, Wiley. b) Schematic description of the microinjector operation. Reproduced with permission.^[77] Copyright 2018, Elsevier. c) PILLSID operation sequence overview. Reproduced with permission.^[78] Copyright 2021, Science. d) Schematic illustration of on-demand drug release using IMAC and MA. The implanted IMAC releases liquid drugs under magnetic actuation of MA. Reproduced with permission.^[79] Copyright 2023, Elsevier. e) Schematic illustration of the BEP and the molecular structure of drug-containing oxidized starch (OST). Reproduced with permission.^[80] Copyright 2019, Nature Publishing Group.

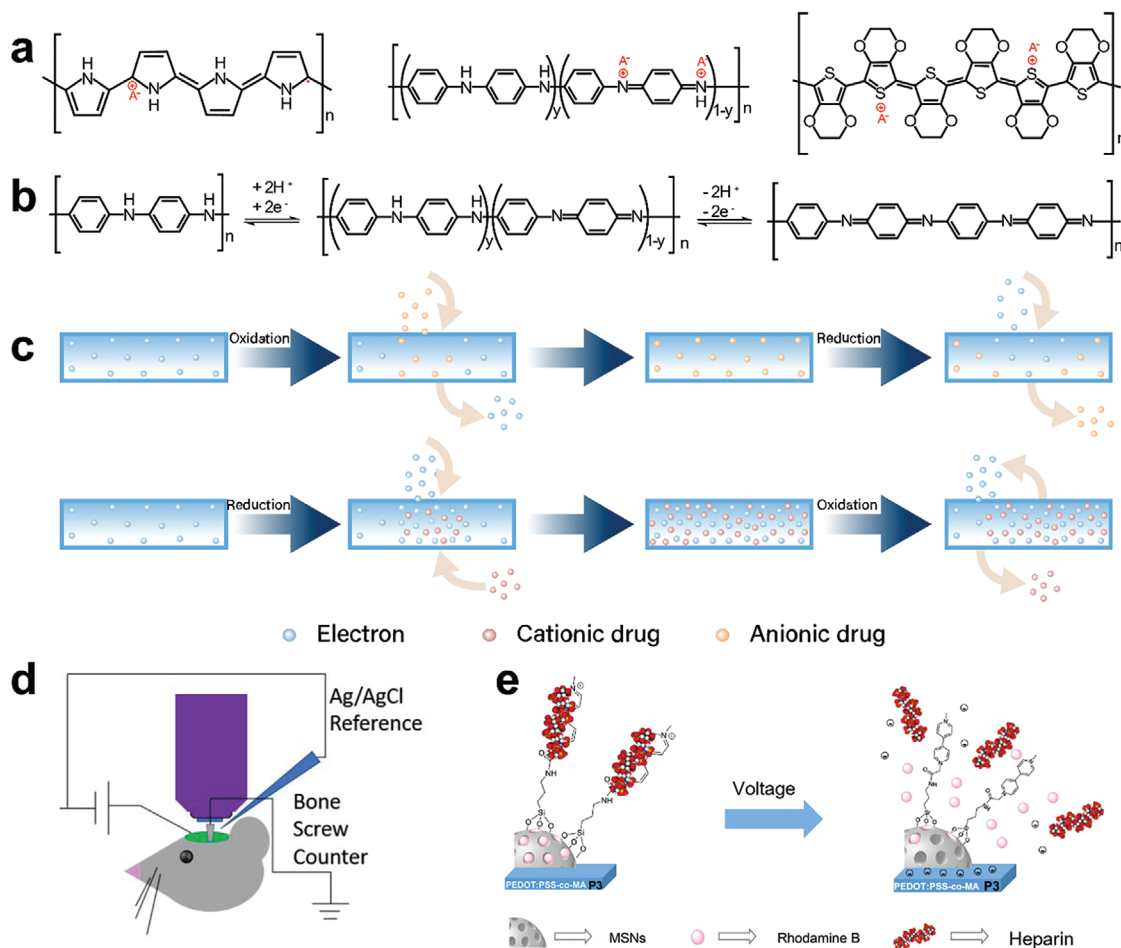


Figure 8. a) Structures of polypyrrole (PPy), polyaniline, and poly (3,4-ethylenedioxythiophene) (PEDOT). b) Transition between different oxidation states of PANI. c) Schematic diagram of the process by which a conductive polymer loads and releases cationic and anionic drugs. d) Schematic diagram of experimental setup for intracranial delivery of DNQX in mice. Reproduced with permission.^[83] Copyright 2019, Wiley. e) Rhodamine release process from PEDOT film. Reproduced with permission.^[84] Copyright 2020, Elsevier.

power the implantable drug reservoir, turning on the drug release.^[82]

3.5. Electro-Responsive IDDS

Electro-responsive IDDSs offer unique advantages because the intensity, direction, and other parameters of electricity are easily and accurately controlled by programming, making the drug release system more accurate and reliable. In addition, the power management system can be integrated into a microchip and combined with smart materials to build a closed-loop micro-DDS with a sensing function that can provide the physiological status, drug dosage, and other information to patients via electromagnetic signals to adjust the release mode. This lays the foundation for precision medicine.

An electro-responsive IDDS mainly consists of a power-supply system and drug-loading system. Drug carriers are usually conductive polymers, conductive hydrogels, metal nanoparticles, and carbon-based nanomaterials.^[85] Conductive polymers and conductive hydrogels are the most commonly used materials.

Conductive polymers are polymeric materials with high electrical conductivity and biocompatibility. Conductive polymers have been considered as potential candidates for drug delivery systems since the 1980s, when Zinger and Miller demonstrated that applying a voltage could release glutamate and ferrocyanide from polypyrrole films.^[86] The first conductive polymers discovered were polyacetylene, and more than 25 conductive polymers have been used in drug delivery after more than 40 years of research and development.^[87] Among these, polypyrrole (PPy), poly (3, 4-ethylenedioxythiophene) (PEDOT) and polyaniline are the most widely used (Figure 8a). PPy and PEDOT are members of the polyheterocyclic family of conductive polymers, which have good biocompatibility and have been proven to be non-toxic to fibroblasts, endothelial cells, and mesenchymal stem cells.^[88] Polyaniline and oligo-aniline have convertible oxidation states (leucoemeraldine, emeraldine, and pernigraniline bases), which provide electrical response properties for polyaniline and oligo-aniline based biomaterials (Figure 8b). In addition, polyaniline and oligo-aniline release acidic ions and adsorb bacteria via electrostatic interactions. This inherent antibacterial ability makes it advantageous for wound healing and other fields.^[89]

Hydrogels are polymers with a three-dimensional (3D) network structure that can absorb a large amount of water and expand. Because their properties are similar to those of extracellular matrices, hydrogels have been widely used in biomedical fields, including tissue engineering, drug delivery, and biosensors.^[90] However, the poor mechanical strength and electrical conductivity of pure hydrogels limit their applications. Conductive hydrogels can be prepared by introducing conductive components into a pure hydrogel, which offers the advantages of both conductive polymers and hydrogels. These conductive components can be conductive polymers, metal nanoparticles, carbon-based nanomaterials, etc.^[91] The introduction of conductive components not only improves the conductivity of hydrogels, but also endows them with new properties, such as strong mechanical properties, stimulus responsiveness, and self-healing ability, which greatly expands the application scope of hydrogels.

The release mechanisms of electrically responsive DDSs include reversible redox reactions of the carrier, or pH changes induced by water electrolysis, and changes in the carrier pore size or hydrophilic/hydrophobic state caused by electrical stimulation. The release process is usually a combination of various mechanisms, and it is difficult to determine the main driving force. Some representative studies were selected to elaborate on the main mechanisms.

3.5.1. IDDS Based on Reversible Electrochemical Redox Reaction

Conductive polymer is a typical example of a drug release mediated by reversible redox reactions. The backbones of conductive polymers have π -conjugate structure, and the delocalized π electrons are able to move on chains, and act as charge carriers to give the polymer electrical conductivity. Conductive polymers are usually synthesized in an oxidized state and require negatively charged dopants to maintain the charge balance and stabilize the backbone. When a negative potential is applied, the backbones are reduced, and the electrostatic interaction between the backbones and dopants is destroyed, leading to the expulsion of the dopants, whereas the opposite is true when a positive potential is applied. Similarly, cationic drugs were doped in the conductive polymers reduction state and released in the oxidation state (Figure 8c). Bansal et al. incorporated polypyrrole into a methacrylate gelatin hydrogel for the controlled release of glutamate. When a reduction potential was applied, the negative charges on the backbone increased, and electrostatic repulsion was generated to expel glutamate from the carrier.^[92] Positively charged drug is released when conductive polymers are oxidized. For example, Ge et al. loaded positively charged daunorubicin onto PPy nanoparticles. Under an oxidation potential, PPy was oxidized, the positive charge on the main chain increased, and daunorubicin was released through electrostatic repulsion.^[93] The reversible redox nature of conductive polymers has also been used to simultaneously release drug molecules with opposite charges. Woeppl et al. incorporated sulphonate modified silica nanoparticles (SNP) into PEDOT films with a drug loading capacity of 0.55 g cm^{-3} , which could simultaneously load and release drugs with opposite charges, such as rhodamine and fluorescein. The stimulated release of fluorescein and rhodamine in the silica nanoparticles was 6.4 times and 16.8 times

higher than in the group without silica nanoparticles. In addition, it protects melatonin from oxidative inactivation during electrochemical polymerization. Then, the PEDOT/SNP-loaded glutamate alpha-amino-3-hydroxy-5-methyl-4-isoxazolepropionic acid (AMPA)/kainate receptor DNQX was polymerized on a carbon fiber electrode and implanted into the brains of GCaMP mice (Figure 8d). DNQX is released after electrical stimulation and significantly inhibits the production of action potentials by mouse neurons. This demonstrates the feasibility of the IDDS in controlling drug release.^[83]

The release of drugs depends on changes in the static charge of the carriers. Compared with a simple sustained-release system, the amount of drug leakage was significantly reduced, and the release dose was more controllable. However, it is only suitable for therapeutic molecules with specific charges, and cannot be applied to neutral molecules. Therefore, it is important to design a controlled-release system that is not limited by the charge properties of the therapeutic agent. Paun et al. designed an electrically responsive microreservoir array consisting of miniature drug storage pools. Dexamethasone was dissolved in a phosphate buffer solution, mixed with glycerol to increase its viscosity, mixed with PPy nanoparticles, and added to microreservoir. When an oxidation potential was applied, the positive charge on the PPy backbone increased and anions in the medium entered the PPy nanoparticles, causing expansion, creating pressure, and pushing the drug solution out. The degree of proliferation of the MG-63 osteoblasts on the surface of the system was similar to that of the control group, indicating no cytotoxicity. Within 350 h, the microreservoir delivered 98% and 30% of the drug with and without electric field stimulation, respectively.^[94] García-Fernández et al. mixed porous silica microspheres loaded with Rhodamine B into PEDOT films and closed the pore outlet with positively charged heparin (PEDOT: PSS-co-MA). Upon electrical stimulation, heparin detached from the pores, leading to the release of Rh B (Figure 8e).^[84] In addition, the expansion or contraction of carriers, mediated by redox reactions, is the driving force for drug release. For example, in the electrochemical pump designed by Yan et al., the electrode was a polycaprolactone-block-polytetrahydrofuran-block-polycaprolactone (PPy/PCTC) composite film. Under electrical stimulation, PPy was oxidized and a large number of anions in the PBS solution entered the film, resulting in a stronger attraction between PCTC and PPy, leading to film contraction. When PPy was reduced, the anions were expelled, and PCTC separated from PPy. However, it remains in the PPy frame, causing the film to expand and infuse the drug.^[95] Systems triggered by structural deformation are not limited by the inherent properties of the drug but also protect the payload from environmental damage.

In addition to conductive polymers, certain metal ions exhibit reversible redox properties. These ions often chelate polysaccharides, such as sodium alginate and chitosan, to form ion hydrogels. The stability of hydrogels formed by ions of different valence states varies, which provides a new idea for the design of electrically responsive DDSs. For example, Ambrozic et al. designed an electrically responsive DDS to control the release of bovine serum albumin (BSA) using a ferric ion-cross-linked alginate gel. The gelation process is caused by the chelation of ferric ions and carboxyl anions by alginate. The chelation of Fe^{2+} with

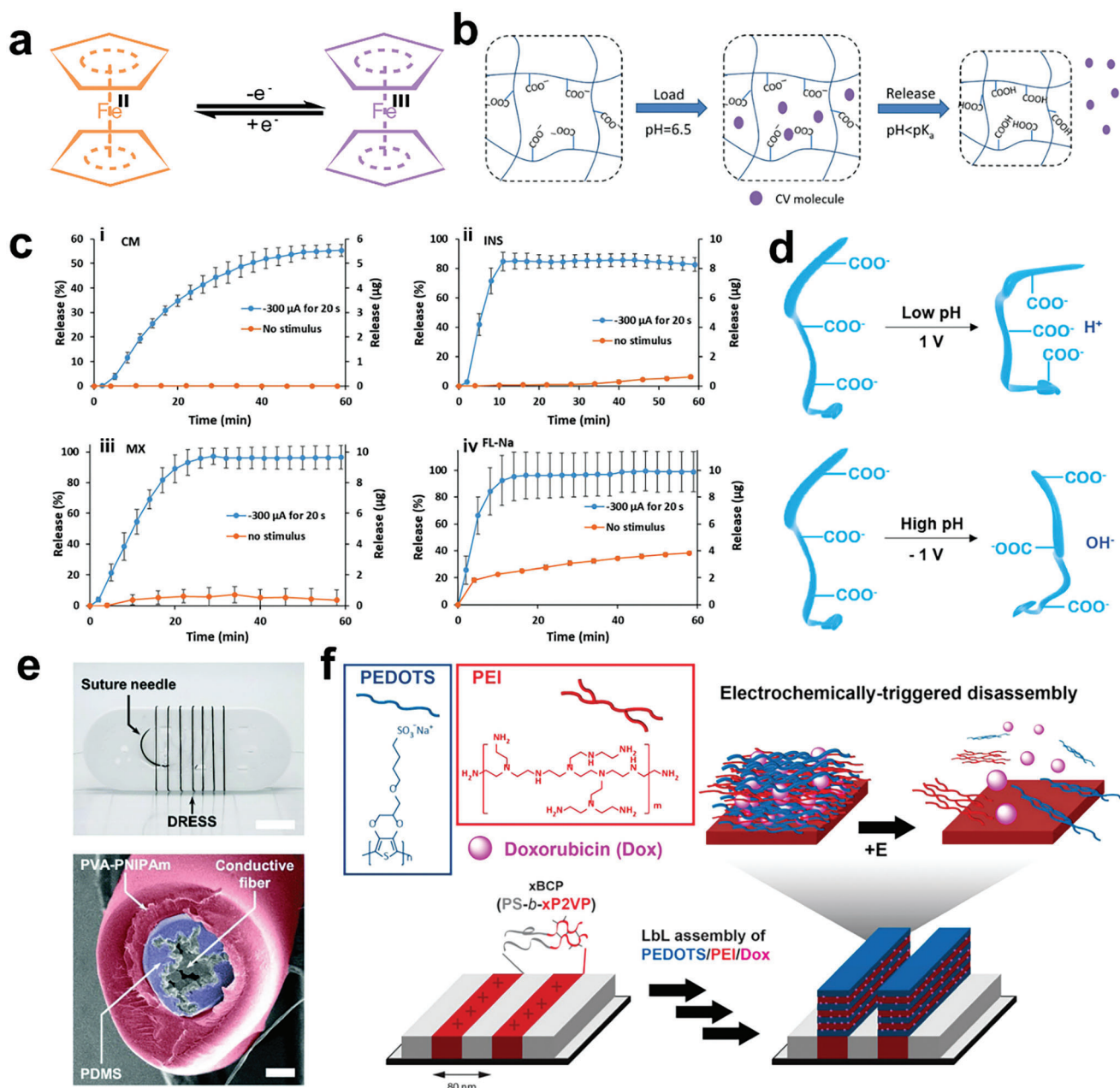


Figure 9. a) Reversible REDOX reaction of ferrocene. b) CV is loaded into the pNIPAm-co-AAc microgels at high pH through electrostatic interactions. When the microgels are neutralized, the CV can be released. Reproduced with permission.^[99] Copyright 2018, The American Chemical Society. c) Pulsed release and leakage with $-300 \mu\text{A}$ for 20 s each of (i) CM, (ii) INS, (iii) MX, and (iv) FL-Na with P5 as carrier-polymer. Reproduced with permission.^[31] Copyright 2018, The Royal Society of Chemistry. d) Effect of pH and electrical stimuli on the alginate chain. Reproduced with permission.^[100] Copyright 2020, The American Chemical Society. e) An optical image (up, scale bars, 10 mm) and a cross-sectional scanning electron microscope (SEM) image (down, scale bars, 100 μm) showing the structure of DRESS. Reproduced with permission.^[101] Copyright 2021, The Royal Society of Chemistry. f) Components and scheme of the layer-by-layer assembly of PEDOTS/PEI/Dox on the nanopatterned xBCP substrate. Reproduced with permission.^[102] Copyright 2020, The American Chemical Society.

alginate was much less stable than that of Fe^{3+} . When Fe^{3+} is reduced to Fe^{2+} , the gel transforms into a sol, releasing BSA. In contrast, oxidative potential prevented the release of BSA.^[96] Ferrocene (Fc) is an organic metal complex with interlayer structure and reversible redox properties. The orange hydrophobic neutral Fc can be oxidized to purple hydrophilic cationic Fc. Under the

reduction potential, it returned to the initial state (Figure 9a). Therefore, Fc is often used as a redox response center to prepare smart DDSs.^[97] Chang et al. used a ferrocenyl surfactant and amphiphilic poly(ethylene glycol)-*b*-poly(acrylic acid) (PEG₁₁₃-*b*PAA₃₀) to prepare a voltage-responsive superamphiphilic polymer (PEG₁₁₃-*b*PAA₃₀/FTMA). In the reduced state, when the

micelle concentration exceeded the critical aggregation concentration ($c_{ac,ed}$), PEG₁₁₃-BPAA₃₀/FTMA self-assembled into spherical micelles. Under voltage stimulation, Fc is oxidized to a hydrophilic ion state, which causes the micelles to disintegrate and release rhodamine 6G. Changes in PEG₁₁₃-bPAA₃₀/FTMA from spherical to irregular fragments were observed using TEM. If the micelle concentration in the oxidized state was higher than that in the $c_{ac,ox}$, the micelles would not disaggregate under voltage stimulation, but the particle size would increase to 40–120 nm. When a reduction potential was applied, the micelles returned to their original state (20–30 nm). The degree of micelle disintegration is related to the degree of oxidation, which can be controlled by voltage.^[98]

3.5.2. IDDSs Based on Water Electrolysis

Under electrical stimulation, water electrolysis causes a change in the pH near the electrode, triggering drug release. A decrease in anodic pH is usually accompanied by proton depletion. Xu et al. deposited a monolithic layer of poly(N-isopropylacrylamide-co-acrylic acid) (pNIPAm-co-AAc) on an anode and loaded it with crystal violet. When the electrolysis of water caused the pH near the anode to drop below 4.25, the acrylic anions accepted protons and became electroneutral, resulting in the disappearance of electrostatic interactions between the microgel and crystal violet, which led to the release of crystal violet (Figure 9b). The microgel could be reloaded by immersion in a crystal violet solution, indicating that the drug-loaded electrodes could be reused.^[99] An increase in pH at the cathode usually causes carrier deprotonation or dissolution to release the cargo. Neumann et al. used methacrylic acid and a methyl methacrylate copolymer to encapsulate FITC-labeled insulin (FITC-INS), meloxicam (MX), fluorescein sodium (FL-Na), and curcumin and deposited them on the cathode surface. Electrical stimulation can increase the pH near the cathode, and the copolymer dissolves and releases the load. Under -300 μ A current stimulation, FITC-INS, MX and FL-Na released 82%, 92% and 99%, respectively. Without electrical stimulation, cargo release depends on its water solubility. For example, the amount of hydrophilic fluorescein sodium released was 32% within 60 min, whereas hydrophobic curcumin showed almost no leakage (Figure 9c).^[31] Puiggali-Jou et al. incorporated PEDOT and polystyrene sulfonate (PSS) into alginate gels loaded with curcumin. After applying electrical stimulation, cathodic alkalinity enhancement resulted in deprotonation of the carboxyl groups on the gel. Electrostatic repulsion between the carboxyl anions causes gel expansion, releasing curcumin (Figure 9d). Without voltage stimulation, the release amount of curcumin was only $3.3\% \pm 1.0\%$ after immersion in the release medium for 9 days, while under -0.1 V voltage stimulation, the release amount was up to 25% within only 2 h.^[100] Zhu et al. synthesized PPy nanoparticles and deposited it on graphene electrodes after loading fluorescein. Under -1.5 V voltage stimulation, water electrolysis led to OH⁻ generation near the electrode, which deprotonated and negatively charged PPy. The electrostatic repulsion forces between the negative PPy and fluorescein could push out fluorescein and simultaneously cause changes in the PPy structure (expansion or contraction). The release of fluorescein from the electrode was significantly higher at -1.5 V compared with

+1.5 V and 0 V. Moreover, cell assays showed no obvious cytotoxicity, indicating the good biosafety of this system.^[103]

H₂ and O₂ produced by the electrolysis of water also act as signals that trigger cargo release. In a closed drug-loading cell, gas generation can exert pressure on the cargo. For example, Song et al. designed a pressure pumping system consisting of a drug storage chamber, catheter, diaphragm, and an electrochemical power chamber from top to bottom. The electrolysis of water produces H₂ and O₂, which increase the chamber pressure, causing the diaphragm to bulge upward and extricate the drug solution from the drug storage chamber. Bubbles from water electrolysis were clearly visible under a voltage of 3 V, and the amount of drug administered was almost linearly proportional to the voltage used and the time of voltage application.^[111] This system separates the electrochemical reaction from the drug-loading pool, avoiding the electrochemical inactivation of drugs. In addition, drug preparations can be repeatedly filled, allowing long-term, precise, and controlled release.

3.5.3. IDDS Based on Electro-Controlled Expansion and/or Contraction of Carriers

The controlled release of hydrogel-based drugs usually involves swelling and deswelling mechanisms. Applying an electric field can cause counterions in the release medium to enter or exit the gel, which may change the charge of the active functional groups on the gel and generate electrostatic repulsion or attraction, causing gel expansion or contraction. In addition, the electrostatic interaction between the electrode and gel is responsible for the change in the gel structure. For example, Paradee et al. introduced poly(2-ethylaniline) into dextran hydrogels to encapsulate diclofenac disodium (Dcf). The pore size of the gel with the same crosslinking ratio increased under voltage stimulation. The pore size of gel with cross-linking ratio of DX500K_0.2STMP was increased from $60.43 \pm 7.88 \mu\text{m}$ to $67.38 \pm 8.71 \mu\text{m}$, $80.30 \pm 7.62 \mu\text{m}$ and $95.87 \pm 10.60 \mu\text{m}$ after applying voltage of 0.5, 1, and 3 V, respectively. Correspondingly, the release amount of Dcf was increased from 2.31 mg (28.7%) to 7.92 mg (98.61%) when the voltage increased from 0 and 3 V.^[104] In addition to hydrogels, thermosensitive polymers can also control drug release through structural changes. Lee et al. prepared a conductive fiber core containing silver nanoparticles, and the outer layer was coated with a drug-loaded thermosensitive polymer-polyvinyl alcohol-grafted N-isopropyl acrylamide (PVA-PNIPAm) for wound closure (Figure 9e). Upon stimulation with a voltage of 130 mV, heat generation from the fiber core caused the PVA-PNIPAm to shrink, pushing out the drug. By optimizing the ratio of PVA to PNIPAm, the cargo release rate of the experimental group was increased by $98.2 \pm 19.5\%$. In the scratch assay in vitro, compared to the original distance between the two layers of cells, the interlayer distance in the electrical stimulation group was reduced to 11% of the original distance, while the control group retained 31% of the original distance. These cells remain highly activated.^[101]

3.5.4. Other Electro-Responsive IDDS

The use of multilayer conductive polymers for drug delivery is a fast-response strategy. A multilayer polymer film system is

assembled layer-by-layer on a bulk substrate through electrostatic interactions between the charged drug and the oppositely charged film. Its structure and charge properties change periodically and its electrical response speed is fast, which is conducive to cargo incorporation. Shen et al. designed a drug delivery system with a substrate composed of polystyrene-block-poly(2-vinyl pyridine) (PS-*b*-Xp2VP), in which polystyrene was electrically neutral, xP2VP was positively charged, and the two fragments were arranged alternately (Figure 9f). On top of the substrate, PEDOT, poly(ethylene imine) (PEI), and DOX appeared alternately and were assembled layer by layer to form a stereoscopic structure (PEM). After applying the oxidation potential, PEDOT was oxidized, the electrostatic attraction between PEDOT and PEI was destroyed, and the assembly disintegrated to release DOX.^[102]

Similar to photolysis, electrical stimulation can cleave the chemical bonds between carriers and drugs to trigger drug release. Hou et al. attached aniline to the surface of graphene and loaded 9-anthracenecarboxaldehyde to form a Schiff base between the amine groups and drug molecules. Under 1.35 V voltage, 43% and 62% of the drug was released within 10 and 120 s, respectively. ¹H NMR analysis of the product showed that 9-anthracenecarboxaldehyde was the main component, and there was a small amount of the oxidation product.^[105]

4. Self-Powered IDDS

As discussed above, electro-responsive IDDS offer many advantages for achieving superior controlled release performance. However, one of the major challenges in electro-responsive IDDS is the energy supply. Traditional batteries for implantable electronic devices have the limitations of potential biosafety hazards and battery capacity, exposing patients to the risk of leakage, and burdening them with multiple surgeries to replace the batteries. Recently, new self-powered technologies have been reported to power IDDS, including triboelectric nanogenerators (TEENG) and enzyme biofuel cell (EBFCs) technologies.

4.1. TENG-Powered IDDS

TENG, invented by Professor Zhong Lin Wang in 2012, can convert mechanical energy into electrical energy based on the coupling effects of triboelectrification and electrostatic induction. It has four operating modes: vertical contact-separation mode, lateral sliding mode, single-electrode mode, and freestanding triboelectric layer mode. Consider a single-electrode TENG operating in the contact and separation modes as an example. Electrodes with strong and weak electron-binding abilities are referred to as electret materials and electrodes, respectively. When the two materials come into contact, the electret material gains electrons from the electrode and possesses these charges quasi-permanently. As they are separated, electrons flow from the back electrode of the electret material to the ground through the external circuit due to electrostatic induction, thus generating a current in the circuit. When the two materials come into contact again, the electron flow is reversed (Figure 10a).^[106] The output of the TENG is closely related to the difference in the electron binding ability between the two electrode materials.

The development of TENG has led to the development of several self-powered biomedical devices that can convert biomechanical energy into electricity. The early application of TENG in biomedical devices was for human health monitoring. However, before 2014, TENG had several disadvantages in biomedical applications, such as a low degree of fit and uncomfortable wearing.^[32] In April 2014, Zhong et al. integrated a TENG into fibers to design a soft and comfortable fabric sensor (FBG) (Figure 10b,c).^[107] After that, several soft and flexible TENG were developed. Zheng et al. designed an implantable TENG to capture the energy of the heartbeat in the body and convert it into electricity, which can be used to monitor the heart rate (Figure 10d).^[108] The device was then integrated with a surgical catheter to create an endocardial pressure sensor that could be minimally implanted to monitor arrhythmia (Figure 10e).^[109] Ryu et al. implanted a TENG at the back of an adult hybrid dog, and the output of the TENG reached 4 V under laboratory conditions. Subsequently, the concept of integrating a TENG with a cardiac pacemaker was proposed, and the pacing mode was verified.^[110]

With the deepening of research, the output performance of TENG has been greatly improved, and their application in the biomedical field has gradually expanded, including tissue regeneration,^[111] cancer treatment,^[112] intracellular drug delivery,^[113] and antibacterial agents.^[114] For example, Liu et al. designed an electroporation platform based on a nanoneedle array electrode and disk TENG. The voltage (20 V) generated by the disk-type TENG produced an electric field of up to 2800 V cm⁻¹ at the nanoneedle tip, which could efficiently deliver foreign molecules to different types of cells.^[113] In order to meet the needs of processing a large number of cells in practical applications, Liu et al. designed a high-throughput electroporation device with a one-dimensional (1D) nanostructure and a multilayer TENG.^[115]

Recently, self-powered drug delivery systems integrating TENG, including transdermal and implantable drug delivery systems (IDDSs), have received considerable attention. Ouyang et al. designed a radial-array rotary TENG to drive the transdermal administration of dexamethasone sodium phosphate (DEX-P⁻) in PPy films. The output voltage of the TENG can reach 250 and 100 V with motor driving and manual rotation, respectively. For the drug release testing, a power management unit was used to modulate the TENG output, and the voltage was constant between 0.8–1.1 V. In a 60 min release test, the TENG-driven drug release curve was similar to that at the same level of potentiostat stimulation. In vitro experimental results showed that the performance of this system was 50% higher than that of traditional transdermal patches.^[116] More recently, we designed a contact-separation TENG-powered iontophoresis transdermal drug delivery system that promoted the subcutaneous penetration of drugs. The TENG can be integrated into insoles, offering a promising solution for self-powered wearable systems by converting biomechanical energy into electrical energy (Figure 11a). The resulting voltage generated an electric field between the electrodes, which accelerated the penetration of rhodamine 6G and methylene blue (MB) into the skin through electrophoresis (Figure 11b).^[117] In order to enhance the transdermal drug delivery of macromolecules drugs and nanomedicines, we developed a wearable self-powered microneedle patch that integrates a

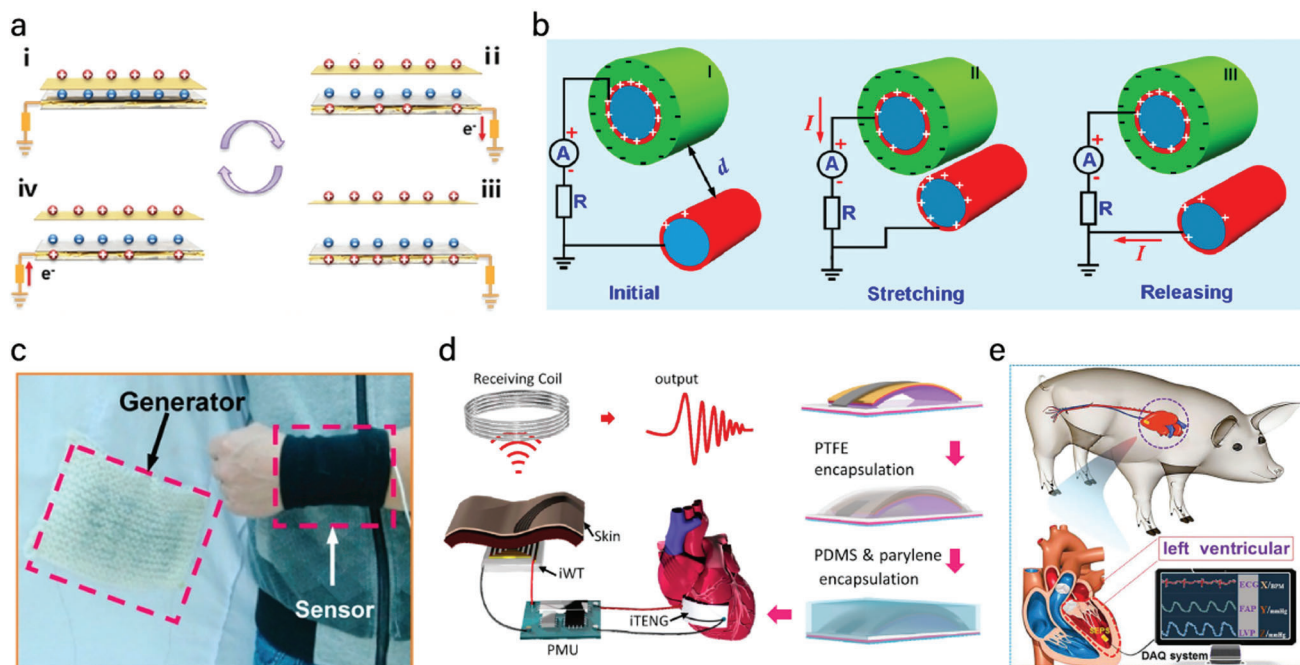


Figure 10. a) Schematic diagram of generator mechanism for the single electrode TENG working under contact and separation mode. Reproduced with permission.^[106] Copyright 2022, Wiley. b) Power generation mechanism of the FBG and c) digital photograph of a wireless body temperature monitor system triggered by the power clothes. Reproduced with permission.^[107] Copyright 2014, The American Chemical Society. d) Schematic diagram of iTENG's construction and heart rate monitoring. Reproduced with permission.^[108] Copyright 2016, The American Chemical Society. e) Schematic diagram of the semaphore acquisition from the TENG implanted into an Adult Yorkshire swine's heart. Reproduced with permission.^[109] Copyright 2019, Wiley.

flexible TENG. Because of the advantages of both microneedles and TENG, therapeutic nanoparticles can penetrate deep into the skin upon microneedle patch insertion (Figure 11c).^[118]

The unique characteristics of the TENG make it well-suited as a “perfect” long-life power source for implantable devices. Song et al. designed an IDDS controlled using TENG-powered water electrolysis. A rotating single-electrode TENG with stable outputs of 15 V, 1.5 mA was fabricated to initiate water electrolysis. The drug carrier pool was prepared using PDMS, which contained two chambers separated by a membrane. The bottom chamber contained water and a pair of patterned electrodes, and the top chamber contained a drug solution. The voltage generated from the TENG triggered water electrolysis to produce H₂ and O₂, creating high pressure to squeeze out the drug solution (Figure 11d). Under 300 and 600 rotating of TENG, the pumping flow rates reached 5.3 and 40 $\mu\text{L min}^{-1}$, respectively. The infusion tube was implanted under the sclera of a pig eye to deliver the fluorescent dye, and significant fluorescence was observed in the anterior chamber of the pig.^[119] Wang et al. combined a TENG with a piezoelectric effect to design a flexible hybrid self-driving system, which was combined with a conductive hydrogel for electrical stimulation to regenerate bone defects. The hybrid generator was implanted into the subcutaneous tissue of the rats, and biphasic electric pulses were generated. The pulses form a bioelectric field in the conductive hydrogel filled with bone defects and induce various biological processes to promote defect repair.^[120] Yao et al. designed a TENG based on LiCl solution to trigger NO release as an adjunct therapy for gliomas. The surface-wearable TENG con-

sists of a LiCl solution encapsulated in PDMS (wsTENG). The open-circuit voltage of the wsTENG is 401 V at an operating frequency of 1 Hz. Electricity from the TENG lit up an LED with blue light (455–465 nm) to trigger NO release, killing C6 glioma cells and 4T1 cells.^[112b]

4.2. Enzyme Biofuel Cells (EBFCs)

Biofuel cells (BFCs) use biocatalysts to convert the biochemical energy from organic matter into electricity. BFCs are primarily composed of biological anodes and cathodes. At the anode, biocatalysts catalyze substrate oxidation. Electrons are transferred directly or indirectly to the electrode and then flowed to the cathode through an external circuit. Under the action of the cathode biocatalysts, the substrate receives electrons and is reduced. Because the enzymes are not lost during the process of catalyzing the reaction, BFCs can theoretically generate a steady current when the substrate is sufficient. Based on the biocatalyst used, BFCs can be divided into three categories: Microbial fuel cells (MBFCs), organelle biofuel cells (OBFCs), and enzyme biofuel cells (EBFCs). MBFCs use microorganisms as catalysts and are primarily used for sewage treatment and power generation. OBFCs use organelles as catalysts.^[121] As organelles contain many enzymes, their substrate selectivity is poor. EBFCs use enzymes as catalysts and have higher catalytic efficiencies and rates than MBFCs. With the development of enzyme immobilization technology, EBFCs have been applied in various fields, such as environmental engineering (sewage treatment and

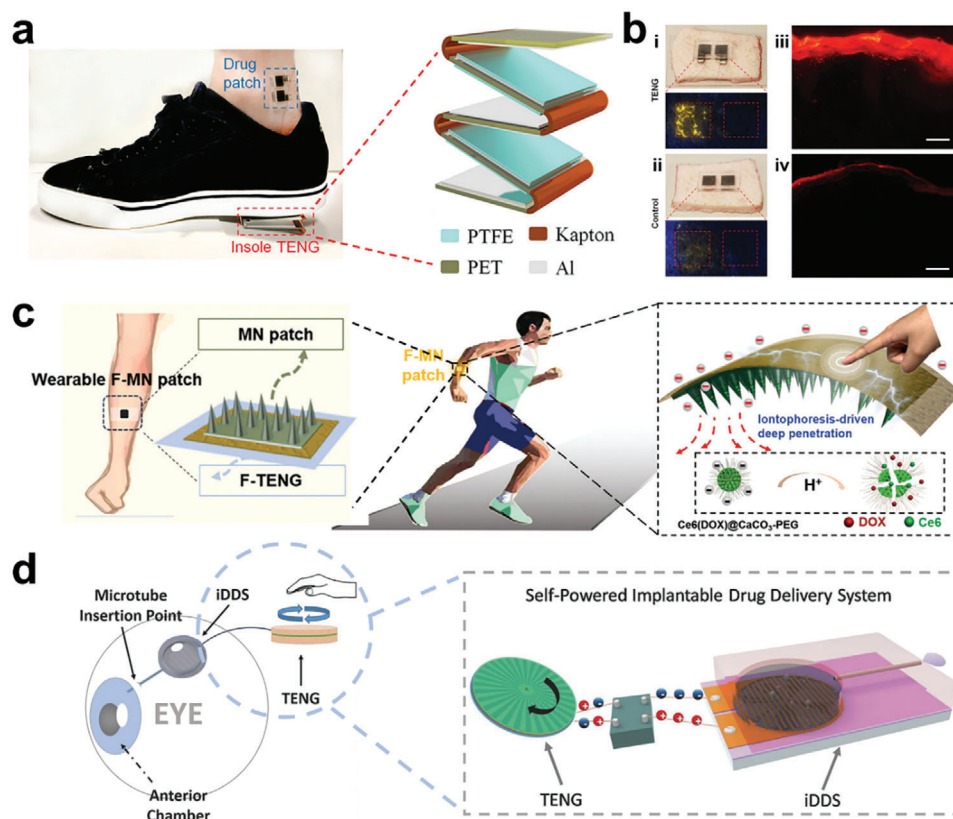


Figure 11. a) Photograph of the ideal wearable drug delivery system on a human ankle, the insert is the schematic of the insole TENG. b) Photograph of the R6G-containing hydrogel drug patch on skin (left) and the fluorescent cross-sectional histological images (right). Scale bar, 50 μm . Reproduced with permission.^[117] Copyright 2020, Wiley. c) Schematic diagram of a wearable F-MN patch.^[118] Copyright 2023, Wiley. d) Schematic illustration of the TENG-based iDDS for drug delivery in the anterior chamber. Reproduced with permission.^[119] Copyright 2017, Wiley.

carbon capture) and biomedicine (biosensing and implantable power devices).^[122]

Enzymes possess favorable attributes for use in physiological environments because of their mild working environment, high catalytic efficacy, and high selectivity. In conjunction with the significant advancements in enzyme immobilization techniques, EBFCs have garnered considerable interest in the field of biomedicine. Similar to TENG, EBFCs also hold potential for the development of self-powered wearable and implantable biosensors or DDS. Glucose, lactic acid, and pyruvate are frequently employed as substrates for in vitro and in vivo applications, providing a basis for the design of sensors based on tears, sweat, and blood.^[123] The output of implantable EBFCs is generally low, and their half-life is short because biological molecules such as proteins in body fluids are easily adsorbed onto EBFCs, forming mass transfer obstructions and limiting output. Wang et al. designed an EBFCs with maximum power density of $3 \mu\text{W cm}^{-2}$ in human blood, and the half-life was only 2 h.^[124] Gineityte et al. reported an improved glucose dehydrogenase-based EBFCs with average current density of 0.65 mA cm^{-2} at 0.1 V versus SCE and half-life of 4.5 h in blood, but the current decreased to 23% of the initial value after 24 h operation.^[125] To solve this problem, Guo et al. designed a flexible anti-biological pollution fiber, BFC. They modified a hydrophilic zwitterionic anti-biofouling polydopamine-2-methacryloyloxyethyl phospho-

rylcholine layer (PDA-MPC) onto carbon nanotube fibers to resist the adsorption of nonspecific proteins in complex biological environment. Glucose oxidase (GOx) and platinum on carbon (Pt/C) were selected as the anode and cathode catalysts, respectively, and fixed on modified carbon nanotube fibers (Figure 12a). The maximum power density of the fiber BFC remained above 91% after 100 bending cycles. When implanted in the mouse brain, it produced a power density of $\approx 4.4 \mu\text{W cm}^{-2}$, which remained at $2.5 \mu\text{W cm}^{-2}$ more than a month later. By contrast, the open-circuit voltage of the unmodified electrode decreased below zero after the first day of implantation (Figure 12b). Immunohistochemical staining showed that astroglial and microglial cells did not accumulate around the PDA-MPC-modified electrode one month after implantation, and no neuronal body damage was observed, resulting in a negligible immune reaction (Figure 12c).^[126]

The electricity generated by EBFCs can power the DDS. Xiao et al. designed a self-powered DDS by combining a membraneless glucose/ O_2 EBFC with conductive polymers. EBFCs generate electricity from glucose and O_2 using porous gold nanofilms as electrodes, glucose oxidase (GOx) as the anode catalyst, and bilirubin oxidase (BOx) as the cathode catalyst. The half-life of the EBFC in the buffer solution was 9.2 h. The drug-loaded PEDOT film was deposited on the outermost layer of the cathode, and drug release was closely related to PEDOT reduction.

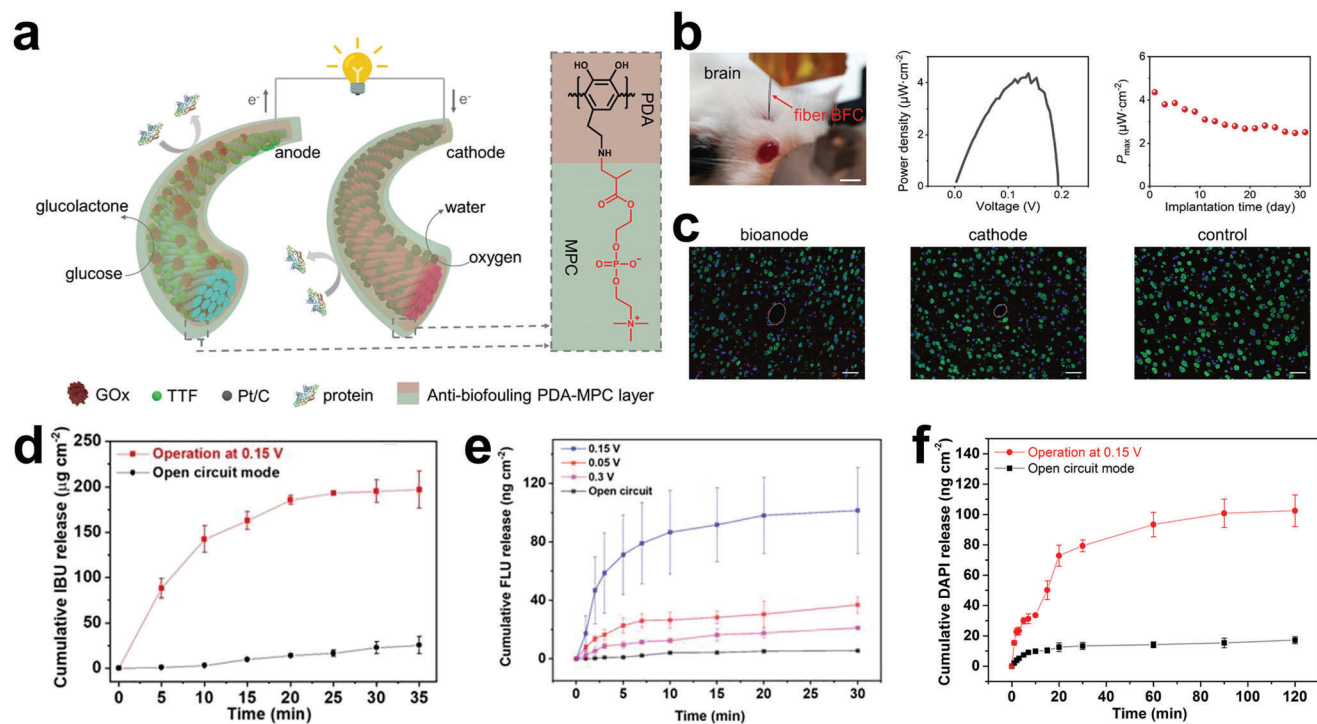


Figure 12. a) Schematic diagram and characterization of fiber BFC. b) left: Photograph showing the implantation of fiber BFC electrode into the mouse brain through sturgeon wire-assisted strategy. Middle: The power density-voltage curve of PDA-MPC modified fiber BFC in the mouse brain on the first day after implantation. Right: The maximal power density of PDA-MPC modified BFC generated in vivo for over a month. c) Immunohistochemical staining images of cross-sectional brain slices at 1 month after implantation of fiber BFC. Reproduced with permission.^[126] Copyright 2022, Wiley. Cumulative amount of d) IBU, e) FLU and f) DAPI released by EBFC (1) operating at 0.15 V. Reproduced with permission.^[127] Copyright 2020, The American Chemical Society.

At 0.15 V, ibuprofen release reached an equilibrium value of $197 \pm 20 \mu\text{g cm}^{-2}$ within 30 min (Figure 12d) and fluorescein release reached an equilibrium value of $101.5 \pm 29.3 \mu\text{g cm}^{-2}$ within 25 min, which was 18 times of spontaneous release (Figure 12e). DAPI release reached an equilibrium value of $102.5 \pm 10.5 \text{ ng cm}^{-2}$ within 90 min, 6 times higher than spontaneous release (Figure 12f).^[127]

Notably, EBFCs often use O_2 as a cathode substrate, which is unsuitable for in vivo applications. Particularly, the output of EBFCs is hindered by the hypoxic tumor environment. Therefore, it is critical to develop EBFCs that can function effectively in hypoxic tumor environments. Jeerapan et al. proposed an internal oxygen supply to overcome this limitation. Oxygen-rich polychlorotrifluoroethylene was used as a cathode material to provide sufficient oxygen for the cathodic reduction reaction.^[128] In addition, short working life, low power density, and unstable output are bottlenecks that limit the development of EBFCs. Currently, improvements can be made in several aspects: a) introducing nanomaterials to increase the amount of enzymes immobilized on the electrode surface and the contact area with the substrate, b) taking protective measures to enhance the stability of enzymes on the electrode surface, and c) accelerating the electron transfer rate between the enzyme and the electrode. EBFCs are environmentally friendly power generation devices and are a promising strategy for using EBFCs to drive medical devices. With the development of EBFCs, a self-powered health-management platform based on EBFCs is expected.

5. “Closed-Loop” IDDS

“Closed-loop” IDDSs can make autonomous decisions about the pattern of drug release. They can detect abnormal physiological signals in the body and spontaneously release appropriate drug doses. A “closed-loop” DDS typically contains three important elements: sensors, control algorithms, and drug delivery systems. Sensors were used to monitor physiological signals and transmit them to the control system. Once the control system determined that the signal exceeded a normal threshold, it sent instructions to the drug delivery system to release the drug. For example, Lee et al. designed a “closed-loop” microbubble enhanced focused ultrasound system for the adjunct treatment of brain cancer. This system has two working modes: imaging and treatment. In the imaging mode, the location of the microbubbles can be monitored by ultrasound imaging. When microbubbles reach the brain, the system detects enhanced echo signals and automatically switches to the treatment mode, adjusting the acoustic emission level, inducing the opening of the blood-brain barrier, and promoting immune adjuvant entry into the brain tumor.^[129]

It is important to note that “closed-loop” DDS are only suitable for diseases with a clear, specific biomarker, such as diabetes, which causes a significant increase in blood glucose. However, for some diseases, such as epilepsy and Parkinson’s disease, there is no clear measurement standard for the severity of the disease, and the symptoms, disease subtypes, and clinical phenotypes are complex and diverse. Therefore, the clinical diagnosis is

highly subjective, and it is difficult to judge whether the disease occurs through a set of fixed control algorithms.^[130] Currently, “closed-loop” DDS systems are mainly used to treat diabetes. Fully automated “closed-loop” DDS are still being studied, and hybrid “closed-loop” systems have been commercialized, such as Medtronic’s 670G, Tandem’s t:slim X2 pump with Control-IQ™, and Insulet’s Omnipod™ 5.^[131] A pilot study used the Medtronic 670G to treat randomly selected adolescents with type 1 diabetes for more than 6 months. Compared with the standard care group, hyperglycemia and blood glucose change indicators were significantly reduced in patients treated with the mixed closed-loop system, and their brain development indicators were more similar to those of healthy people.^[132]

6. Conclusion and outlook

This article summarized the research progress of implantable controlled-release systems. Smart materials with stimulus-responsive capabilities including optical, ultrasonic, electric, and magnetic responses have been used to construct IDDSs in the form of films, patches, micro- and nano-drug storage arrays. In addition, implantable drug-delivery microelectromechanical systems with precise construction have been developed, and patients can interact with them and control the drug release pattern. “Closed-loop” control IDDSs, with built-in sensing and control algorithms, can self-identify abnormal physiological signals and release drugs without human involvement, such that patients, especially those with chronic diseases, can lead a normal life without requiring long-term injections, pills, and tests. Self-powered devices further solve the problem of energy supply for implantable devices, overcoming the limitations of lithium batteries and making them safer and more reliable.

Although the theory and technology of IDDSs have been developed rapidly, several bottlenecks exist for the clinical transformation of IDDSs; a few examples are listed below:

- 1) Some implantable devices inevitably use metallic elements, such as power management systems, coils, and drug storage, which are not biodegradable in the body. A prolonged stay in the body may trigger an inflammatory response, requiring surgical removal of these devices in severe cases.
- 2) Foreign body response remains a problem that limits the function of the IDDSs. Although the biocompatibility of the materials used in IDDSs has improved significantly, they remain heterogeneous relative to the biological tissues; this leads to the formation of dense fibrous capsules at the implant site, hindering the diffusion of the IDDS and its communication with signals outside the body.
- 3) An intelligent IDDS requires complex and delicate structures that challenge its working life and stability in complex physiological environments. The complex structure is easily affected by the surrounding environment, and the pulsation of organs and movement of organisms may cause abnormalities in the IDDS. A precise controlled-release system, especially an IDDS communicating through an electromagnetic field, is easily disturbed by an external electromagnetic field, which causes abnormalities in the IDDS. This problem can be solved by patterning electromagnetic fields. E.g., the induced magnetic field of an IDDS is designed in a special pattern, and

only when a magnetic field corresponding to this pattern is applied, the IDDS can accept the command to initiate working. Abnormalities in automated IDDSs are difficult to detect in time owing to the small amount of human participation. This requires a built-in alarm or a signal indication device when designing an IDDS.

- 4) IDDSs pose new challenges to market regulation and quality control. Because IDDSs have the attributes of both drugs and medical devices, the existing management system may not be fully applicable to IDDSs and needs to be adjusted and improved according to the attributes of IDDSs.

Thus, the increasing focus on personalized medicine, as well as the aging world population and high incidence of cancer and chronic diseases, have led to an increasing demand for medical implants, which provide impetus for governments and companies to increase R&D investment in IDDSs, thereby accelerating the clinical application of the technology.

Acknowledgements

G.H. and H.L. contributed equally to this work. This research was supported by the National Natural Science Foundation of China (22074113, U23A2089, and 22073070), the Young Top-notch Talent Cultivation Program of Hubei Province, Science and Technology Plans of Tianjin (22ZYJDS00070), Postdoctoral Innovative Talents Support Program (BX20230268), and China Postdoctoral Science Foundation (2023M742690).

Conflict of Interest

The authors declare no conflict of interest.

Keywords

controlled release, drug delivery, implantable, response mechanism, stimulus-responsive

Received: November 22, 2023

Revised: February 3, 2024

Published online:

- [1] a) K. Y. Hwa, V. H. S. Chang, Y. Y. Cheng, Y. D. Wang, P. S. Jan, B. Subramani, M. J. Wu, B. K. Wang, *Biomed. Microdevices* **2017**, *19*, 84; b) C. Lo, K. Bhardwaj, R. Marculescu, *Nano Commun. Netw.* **2017**, *12*, 25.
- [2] S. A. Stewart, J. Dominguez-Robles, D. Donnelly, E. Larraneta, *Polymers* **2018**, *10*, 1379.
- [3] T. F. Blaschke, L. Osterberg, B. Vrijens, J. Urquhart, *Annu. Rev. Pharmacol. Toxicol.* **2012**, *52*, 275.
- [4] T. R. Zijp, P. G. M. Mol, D. J. Touw, J. F. M. van Boven, *eClinicalMedicine* **2019**, *15*, 3.
- [5] K. Park, *J. Controlled Release* **2014**, *190*, 3.
- [6] a) R. Jamaledin, C. K. Y. Yiu, E. N. Zare, L. N. Niu, R. Vecchione, G. J. Chen, Z. Gu, F. R. Tay, P. Makvandi, *Adv. Mater.* **2020**, *32*, 2002129; b) D. D. Li, D. D. Hu, H. X. Xu, H. K. Patra, X. R. Liu, Z. X. Zhou, J. B. Tang, N. Slater, Y. Q. Shen, *Biomaterials* **2021**, *264*, 120410.
- [7] a) M. Singhal, C. Serna, V. Merino, Y. N. Kalia, *Eur. J. Pharm. Biopharm.* **2021**, *166*, 175; b) E. A. Takmaz, G. Yener, *J. Drug Deliv. Sci. Technol.* **2021**, *63*, 102438.

- [8] a) C. D. Xu, L. Xu, R. L. Han, Y. B. Zhu, J. F. Zhang, *Colloids Surf., B* **2021**, *201*, 111632; b) Y. Z. Zhang, H. G. Cui, R. Q. Zhang, H. B. Zhang, W. Huang, *Adv. Sci.* **2021**, *8*, 2101454.
- [9] a) H. W. Huh, Y. G. Na, H. Kang, M. Kim, M. Han, T. M. A. Pham, H. Lee, J. S. Baek, H. K. Lee, C. W. Cho, *Int. J. Pharm.* **2021**, *592*, 120113; b) M. Rahamathulla, M. N. Alam, U. Hani, Q. Ibrahim, Y. Alhamhoom, *Pak. J. Pharm. Sci.* **2021**, *34*, 1297.
- [10] M. D. Creinin, R. Jansen, R. M. Starr, J. Gobburu, M. Gopalakrishnan, A. Olariu, *Contraception* **2016**, *94*, 353.
- [11] P. Y. Song, D. Jian, H. Tng, R. Hu, G. Lin, E. Meng, K. T. Yong, *Adv. Healthcare Mater.* **2013**, *2*, 1170.
- [12] J. C. Quarterman, S. M. Geary, A. K. Salem, *Eur. J. Pharm. Biopharm.* **2021**, *159*, 21.
- [13] a) X. L. Li, Y. He, J. W. Hou, G. Yang, S. B. Zhou, *Small* **2019**, *16*, 1902262; b) D. I. Viswanath, H. C. Liu, R. S. Vander Pol, S. Z. Saunders, C. Y. X. Chua, A. Grattoni, *Biomaterials* **2022**, *281*, 121374.
- [14] a) Y. K. Yang, X. Y. Qiao, R. Y. Huang, H. X. Chen, X. L. Shi, J. Wang, W. H. Tan, Z. K. Tan, *Biomaterials* **2020**, *230*, 119618; b) C. T. Hagan, C. Bloomquist, S. Warner, N. M. Knape, I. Kim, H. Foley, K. T. Wagner, S. Mecham, J. DeSimone, A. Z. Wang, *J. Controlled Release* **2022**, *344*, 147.
- [15] X. Y. Xu, C. Liu, Y. H. Wang, O. Koivisto, J. N. Zhou, Y. L. Shu, H. B. Zhang, *Adv. Drug Delivery Rev.* **2021**, *176*, 113891.
- [16] a) K. Yu, X. Y. Yang, L. H. He, R. Zheng, J. Min, H. Y. Su, S. Y. Shan, Q. M. Jia, *Polymer* **2020**, *200*, 122585; b) W. D. Xu, J. L. Wang, Q. H. Li, C. H. Wu, L. L. Wu, K. Q. Li, Q. Li, Q. Han, J. J. Zhu, Y. H. Bai, J. J. Deng, J. Lyu, Z. Wang, *J. Mater. Chem. B* **2021**, *9*, 8031; c) J. L. Gao, Z. Qiao, S. Liu, J. X. Xu, S. Wang, X. Yang, X. Wang, R. P. Tang, *Eur. J. Pharm. Biopharm.* **2021**, *163*, 188.
- [17] D. Sarmah, M. A. Rather, A. Sarkar, M. Mandal, K. Sankaranarayanan, N. Karak, *Int. J. Biol. Macromol.* **2023**, *237*, 124206.
- [18] F. Y. Lin, N. H. Dimmitt, M. M. d. L. Perini, J. L. Li, C. C. Lin, *Adv. Healthcare Mater.* **2021**, *11*, 2101284.
- [19] G. Wang, J. Y. Gao, Y. K. Fu, Z. H. Ren, J. Huang, X. Li, G. R. Han, *Chem. Eng. J.* **2020**, *388*, 124211.
- [20] S. J. Lu, R. Xia, J. Wang, Q. Pei, Z. G. Xie, X. B. Jing, *ACS Appl. Mater. Interfaces* **2021**, *13*, 46291.
- [21] Q. Pei, X. L. Hu, X. H. Zheng, R. Xia, S. Liu, Z. G. Xie, X. B. Jing, *Nano Res.* **2019**, *12*, 877.
- [22] a) X. X. Shang, Q. Liu, T. Qin, X. D. Xu, H. M. Sun, M. X. Liu, H. D. Zhu, *Int. J. Nanomed.* **2019**, *14*, 3361; b) Y. L. Miao, X. B. Zhao, Y. D. Qiu, Z. Y. Liu, W. J. Yang, X. Jia, *ACS Appl. Bio Mater.* **2019**, *2*, 895; c) C. Conte, P. F. Monteiro, P. Gurnani, S. Stolnik, F. Ungaro, F. Quaglia, P. Clarke, A. Grabowska, M. Kavallaris, C. Alexander, *Nanoscale* **2021**, *13*, 11414.
- [23] Y. J. Yao, J. Ding, Z. Y. Wang, H. L. Zhang, J. Q. Xie, Y. C. Wang, L. J. Hong, Z. W. Mao, J. Q. Gao, C. Y. Gao, *Biomaterials* **2020**, *232*, 119726.
- [24] Z. G. Fu, H. Q. Li, P. Xue, H. Y. Yu, S. Yang, C. Tao, W. Li, Y. J. Wang, J. J. Zhang, Y. Wang, *Front. Bioeng. Biotechnol.* **2022**, *10*, 881544.
- [25] G. H. Lu, G. Zhao, S. Wang, H. Q. Li, Q. Yu, Q. Sun, B. Wang, L. Wei, Z. Fu, Z. Y. Zhao, L. S. Yang, L. F. Deng, X. Y. Zheng, M. Cai, M. Lu, *Adv. Sci.* **2024**, <https://doi.org/10.1002/advs.202306964>.
- [26] Y. Zhou, H. Ye, Y. B. Chen, R. Y. Zhu, L. C. Yin, *Biomacromolecules* **2018**, *19*, 1840.
- [27] S. Talebian, B. Mendes, J. Coniot, S. Farajikhah, F. Dehghani, Z. Y. Li, D. Bitoque, G. Silva, S. Naficy, J. Conde, G. G. Wallace, *Adv. Sci.* **2023**, *10*, 2207603.
- [28] T. Z. Liu, Q. Wan, C. Zou, M. J. Chen, G. Wan, *Chem. Eng. J.* **2021**, *417*, 128004.
- [29] X. B. Wang, F. Y. Yan, X. F. Liu, P. Wang, S. Shao, Y. Sun, Z. H. Sheng, Q. H. Liu, J. F. Lovell, H. R. Zheng, *J. Controlled Release* **2018**, *286*, 358.
- [30] T. Sun, A. Dasgupta, Z. M. Zhao, M. Nurunnabi, S. Mitragotri, *Adv. Drug Deliv. Rev.* **2020**, *158*, 36.
- [31] S. E. Neumann, C. F. Chamberlayne, R. N. Zare, *Nanoscale* **2018**, *10*, 10087.
- [32] H. Wang, J. Cheng, Z. Z. Wang, L. H. Ji, Z. L. Wang, *Sci. Bull.* **2021**, *66*, 490.
- [33] A. N. Khan, A. Ermakov, G. Sukhorukov, Y. Hao, *Appl. Phys. Rev.* **2019**, *6*, 041301.
- [34] C. E. Choi, A. Chakraborty, A. Coyle, Y. Shamiya, A. Paul, *Adv. Healthcare Mater.* **2022**, *11*, 2102088.
- [35] M. Wu, X. Y. Lin, X. H. Tan, J. Li, Z. W. Wei, D. Zhang, Y. S. Zheng, A. X. Zheng, B. X. Zhao, Y. Y. Zeng, *ACS Appl. Mater. Interfaces* **2018**, *10*, 19416.
- [36] S. Karthik, N. Puvvada, B. N. P. Kumar, S. Rajput, A. Pathak, M. Mandal, N. D. P. Singh, *ACS Appl. Mater. Interfaces* **2013**, *5*, 5232.
- [37] J. Q. Jiang, X. Tong, Y. Zhao, *J. Am. Chem. Soc.* **2005**, *127*, 8290.
- [38] T. C. de Souza-Guerreiro, G. Bondelli, I. Grobas, S. Donini, V. Sesti, C. Bertarelli, G. Lanzani, M. Asally, G. M. Paternò, *Adv. Sci.* **2023**, *10*, 2205007.
- [39] H. Q. Zheng, Y. Yang, Z. Y. Wang, D. R. Yang, G. D. Qian, Y. J. Cui, *Adv. Mater.* **2023**, *35*, 2300177.
- [40] a) G. Gao, Y. W. Jiang, H. R. Jia, F. G. Wu, *Biomaterials* **2019**, *188*, 83; b) W. J. Huang, H. Zhao, J. S. Wan, Y. Zhou, Q. B. Xu, Y. B. Zhao, X. L. Yang, L. Gan, *Theranostics* **2019**, *9*, 3825; c) S. P. Liu, Z. C. Liu, M. Y. Wu, X. M. Xu, F. B. Huang, L. Zhang, Y. Liu, Q. Shuai, *Int. J. Biol. Macromol.* **2021**, *191*, 344.
- [41] a) R. G. Fonseca, F. De Bon, P. Pereira, F. M. Carvalho, M. Freitas, M. Tavakoli, A. C. Serra, A. C. Fonseca, J. F. J. Coelho, *Mater. Today Bio* **2022**, *15*, 100325; b) O. Grimm, F. Wendler, F. H. Schacher, *Polymers* **2017**, *9*, 396.
- [42] P. M. Kharkar, R. A. Scott, L. P. Olney, P. J. LeValley, E. Maverakis, K. L. Kiick, A. M. Kloxin, *Adv. Healthcare Mater.* **2017**, *6*, 1700713.
- [43] Q. C. Wei, J. H. Bai, H. Wang, G. L. Ma, X. J. Li, W. W. Zhang, Z. G. Hu, *Carbohydr. Polym.* **2021**, *256*, 117609.
- [44] B. Yan, J.-C. Boyer, D. Habault, N. R. Branda, Y. Zhao, *J. Am. Chem. Soc.* **2012**, *134*, 16558.
- [45] A. Bansal, J. Zhang, Q. Lu, Q. S. Mei, Y. Zhang, *Biomater. Sci.* **2023**, *11*, 2046.
- [46] S. Han, W. Sung, T. Y. Kim, S. J. Yang, S. Kim, G. Lee, K. Cho, S. K. Hahn, *Nano Energy* **2021**, *81*, 105650.
- [47] S. H. Lee, H. Y. Piao, Y. C. Cho, S. N. Kim, G. Choi, C. R. Kim, H. B. Ji, C. G. Park, C. Lee, C. I. Shin, W. G. Koh, Y. B. Choy, J. H. Choy, *Proc. Natl. Acad. Sci. U. S. A.* **2019**, *116*, 11664.
- [48] a) N. M. Salkho, N. S. Awad, W. G. Pitt, G. A. Hussein, *Polymers* **2022**, *14*, 1286; b) H. M. D. Bandara, S. C. Burdette, *Chem. Soc. Rev.* **2012**, *41*, 1809.
- [49] S. J. Leung, M. Romanowski, *Theranostics* **2012**, *2*, 1020.
- [50] a) M. Borowiak, F. Kullmer, F. Gegenfurtner, S. Peil, V. Nasufovic, S. Zahler, O. Thorn-Seshold, D. Trauner, H. D. Arndt, *J. Am. Chem. Soc.* **2020**, *142*, 9240; b) A. Duran-Corbera, J. Catena, M. Otero-Vinas, A. Llebaria, X. Rovira, *J. Med. Chem.* **2020**, *63*, 8458; c) Y. Kim, D. Jeong, V. V. Shinde, Y. Hu, C. Kim, *Int. J. Biol. Macromol.* **2020**, *163*, 824.
- [51] A. Mueller-Deku, J. C. M. Meiring, K. Loy, Y. Kraus, C. Heise, R. Bingham, K. I. Jansen, X. Y. Qu, F. Bartolini, L. C. Kapitein, A. Akhmanova, J. Ahlfeld, D. Trauner, O. Thorn-Seshold, *Nat. Commun.* **2020**, *11*, 4640.
- [52] N. Chander, J. Morstein, J. S. Bolten, A. Shemet, P. R. Cullis, D. Trauner, D. Witzigmann, *Small* **2021**, *17*, 2008198.
- [53] a) Y. Yang, X. Liu, W. Ma, Q. Xu, G. Chen, Y. F. Wang, H. H. Xiao, N. Li, X. J. Liang, M. Yu, Z. Q. Yu, *Biomaterials* **2021**, *265*, 120456; b) X. J. Chen, J. F. Zou, K. Zhang, J. J. Zhu, Y. Zhang, Z. H. Zhu, H. Y. Zheng, F. Z. Li, J. G. Piao, *Acta Pharm. Sin. B* **2021**, *11*, 271; c) L. Xu, S. B. Wang, C. Xu, D. Han, X. H. Ren, X. Z. Zhang, S. X. Cheng, *ACS Appl. Mater. Interfaces* **2019**, *11*, 38385.

- [54] T. X. Chen, Y. Yang, H. Peng, A. K. Whittaker, Y. Li, Q. L. Zhao, Y. Wang, S. M. Zhu, Z. Y. Wang, *Carbohydr. Polym.* **2021**, 266, 118122.
- [55] C. Y. Liu, Z. Y. Wang, X. Y. Wei, B. R. Chen, Y. X. Luo, *Acta Biomater.* **2021**, 131, 314.
- [56] G. Guedes, S. Q. Wang, F. Fontana, P. Figueiredo, J. Lindén, A. Correia, R. J. B. Pinto, S. Hietala, F. L. Sousa, H. A. Santos, *Adv. Mater.* **2021**, 33, 2007761.
- [57] B. Y. Chu, Y. Qu, X. L. He, Y. Hao, C. L. Yang, Y. Yang, D. R. Hu, F. F. Wang, Z. Y. Qian, *Adv. Funct. Mater.* **2020**, 30, 2005918.
- [58] P. F. Sun, T. Huang, X. X. Wang, G. N. Wang, Z. J. Liu, G. S. Chen, Q. L. Fan, *Biomacromolecules* **2020**, 21, 556.
- [59] B. W. Sun, J. N. Bte Rahmat, H. J. Kim, R. Mahendran, K. Esuvaranathan, E. Chiong, J. S. Ho, K. G. Neoh, Y. Zhang, *Adv. Sci.* **2022**, 9, 2200731.
- [60] J. Jin, L. Yang, F. Chen, N. Gu, *Interdiscip. Mater.* **2022**, 1, 471.
- [61] a) Y. N. Dou, K. Hynynen, C. Allen, *J. Controlled Release* **2017**, 249, 63; b) K. Entzian, A. Aigner, *Pharmaceutics* **2021**, 13, 1135.
- [62] D. Q. Huang, X. X. Zhang, C. Zhao, X. Fu, W. J. Zhang, W. T. Kong, B. Zhang, Y. J. Zhao, *Adv. Therap.* **2021**, 4, 2100050.
- [63] T. Kubota, Y. Kurashina, J. Y. Zhao, K. Ando, H. Onoe, *Mater. Des.* **2021**, 203, 109580.
- [64] Y. Zhou, G. T. Liu, S. Y. Guo, *J. Mater. Chem. B* **2022**, 10, 3947.
- [65] Z. Q. Meng, Y. J. Zhang, J. L. She, X. F. Zhou, J. Xu, X. Han, C. Wang, M. F. Zhu, Z. Liu, *Nano Lett.* **2021**, 21, 1228.
- [66] W. X. Sun, H. T. Jiang, X. Wu, Z. Y. Xu, C. Yao, J. Wang, M. Qin, Q. Jiang, W. Wang, D. Q. Shi, Y. Cao, *Nano Res.* **2019**, 12, 115.
- [67] R. Campbell, H. Shim, J. Choi, M. Park, E. Byun, S. Islam, S. H. Song, A. Kim, *Adv. Healthcare Mater.* **2021**, 10, 2001582.
- [68] P. Zhu, Y. Chen, J. L. Shi, *Adv. Mater.* **2020**, 32, 2001976.
- [69] Y. Z. Qiu, S. Tong, L. L. Zhang, Y. Sakurai, D. R. Myers, L. Hong, W. A. Lam, G. Bao, *Nat. Commun.* **2017**, 8, 15594.
- [70] B. D. Cardoso, A. R. O. Rodrigues, M. Banobre-Lopez, B. G. Almeida, C. O. Amorim, V. S. Amaral, P. J. G. Coutinho, E. M. S. Castanheira, *Pharmaceutics* **2021**, 13, 1248.
- [71] A. Rivera-Rodriguez, C. M. Rinaldi-Ramos, *Annu. Rev. Chem. Biomol. Eng.* **2021**, 12, 163.
- [72] G. R. Dai, L. Sun, J. Xu, G. Z. Zhao, Z. Tan, C. Wang, X. L. Sun, K. M. Xu, W. Y. Zhong, *Acta Biomater.* **2021**, 129, 84.
- [73] Y. Wang, G. Boero, X. S. Zhang, J. Brugger, *ACS Appl. Mater. Interfaces* **2022**, 14, 40418.
- [74] M. K. Gupta, J. Bajpai, A. K. Bajpai, *Polym. Eng. Sci.* **2021**, 61, 1427.
- [75] F. C. Lin, J. J. Zheng, W. H. Guo, Z. T. Zhu, Z. Wang, B. Y. Dong, C. S. Lin, B. Huang, B. L. Lu, *Cellulose* **2019**, 26, 6861.
- [76] B. Qian, A. Shen, S. X. Huang, H. P. Shi, Q. Long, Y. M. Zhong, Z. X. Qi, X. J. He, Y. C. Zhang, W. X. Hai, X. M. Wang, Y. N. Cui, Z. H. Chen, H. X. Xuan, Q. Zhao, Z. W. You, X. F. Ye, *Adv. Sci.* **2023**, 10, 2303033.
- [77] S. H. Lee, B. H. Kim, C. G. Park, C. Lee, B. Y. Lim, Y. B. Choy, *J. Controlled Release* **2018**, 286, 224.
- [78] V. Iacovacci, I. Tamadon, E. F. Kauffmann, S. Pane, V. Simoni, L. Marziale, M. Aragona, L. Cobuccio, M. Chiarugi, P. Dario, S. Del Prato, L. Ricotti, F. Vistoli, A. Menciasci, *Sci. Robot.* **2021**, 6, eabh3328.
- [79] Y. Zheng, G. Z. Zheng, Y. Y. Li, X. Gong, Z. P. Chen, L. Y. Zhu, Y. S. Xu, X. Xie, S. Wu, L. L. Jiang, *J. Controlled Release* **2023**, 364, 576.
- [80] J. Lee, H. R. Cho, G. D. Cha, H. Seo, S. Lee, C. K. Park, J. W. Kim, S. T. Qiao, L. Wang, D. Kang, T. Kang, T. Ichikawa, J. Kim, H. Lee, W. Lee, S. Kim, S. T. Lee, N. S. Lu, T. Hyeon, S. H. Choi, D. H. Kim, *Nat. Commun.* **2019**, 10, 5205.
- [81] S. H. Lee, S. H. Min, Y. C. Cho, J. H. Han, M. N. Kim, C. R. Kim, C. H. Ahn, B. H. Kim, C. Lee, Y. M. Cho, Y. B. Choy, *J. Controlled Release* **2020**, 325, 111.
- [82] H. Joo, Y. Lee, J. Kim, J.-S. Yoo, S. Yoo, S. Kim, A. K. Arya, S. Kim, S. H. Choi, N. Lu, H. S. Lee, S. Kim, S.-T. Lee, D.-H. Kim, *Sci. Adv.* **2021**, 7, eabd4639.
- [83] K. M. Woeppel, X. S. Zheng, Z. M. Schulte, N. L. Rosi, X. Y. T. Cui, *Adv. Healthcare Mater.* **2019**, 8, 1900622.
- [84] A. Garcia-Fernandez, B. Lozano-Torres, J. F. Blandez, J. Monreal-Trigo, J. Soto, J. E. Collazos-Castro, M. Alcaniz, M. D. Marcos, F. Sancenon, R. Martinez-Manez, *J. Controlled Release* **2020**, 323, 421.
- [85] Z. Mazidi, S. Javanmardi, S. M. Naghib, Z. Mohammadpour, *Chem. Eng. J.* **2022**, 433, 134569.
- [86] B. Tandon, A. Magaz, R. Balint, J. J. Blaker, S. H. Cartmell, *Adv. Drug Deliv. Rev.* **2018**, 129, 148.
- [87] L. L. Xu, Y. Yang, Y. K. Mao, Z. Li, *Adv. Mater. Technol.* **2022**, 7, 2100055.
- [88] A. Puiggali-Jou, L. J. del Valle, C. Aleman, *J. Controlled Release* **2019**, 309, 244.
- [89] G. X. Zhao, H. W. Zhou, G. R. Jin, B. Jin, S. M. Geng, Z. T. Luo, Z. G. Ge, F. Xu, *Prog. Polym. Sci.* **2022**, 131, 101573.
- [90] Y. Hong, Z. L. Lin, Y. Yang, T. Jiang, J. Z. Shang, Z. R. Luo, *Int. J. Mol. Sci.* **2022**, 23, 4578.
- [91] Z. X. Deng, Y. Guo, X. Zhao, T. M. Du, J. X. Zhu, Y. L. Xie, F. S. Wu, Y. H. Wang, M. Guan, *Gels* **2022**, 8, 280.
- [92] M. Bansal, B. Raos, Z. Aqrave, Z. M. Wu, D. Svirskis, *Acta Biomater.* **2022**, 137, 124.
- [93] J. Ge, E. Neofytou, T. J. Cahill, III, R. E. Beygui, R. N. Zare, *ACS Nano* **2012**, 6, 227.
- [94] I. A. Paun, M. Zamfirescu, C. R. Luculescu, A. M. Acasandrei, C. C. Mustaciosu, M. Mihailescu, M. Dinescu, *Appl. Surf. Sci.* **2017**, 392, 321.
- [95] B. X. Yan, B. Y. Li, F. Kunecke, Z. Gu, L. Guo, *ACS Appl. Mater. Interfaces* **2015**, 7, 14563.
- [96] R. Ambrozic, L. Plazl, *Soft Matter* **2021**, 17, 6751.
- [97] X. Liu, L. Zhao, F. F. Liu, D. Astruc, H. B. Gu, *Coord. Chem. Rev.* **2020**, 419, 213406.
- [98] X. Y. Chang, Z. Y. Cheng, B. Y. Ren, R. F. Dong, J. Peng, S. Y. Fu, Z. Tong, *Soft Matter* **2015**, 11, 7494.
- [99] W. W. Xu, Y. N. Zhang, Y. F. Gao, M. J. Serpe, *ACS Appl. Mater. Interfaces* **2018**, 10, 13124.
- [100] A. Puiggali-Jou, E. Cazorla, G. Ruano, I. Babeli, M. P. Ginebra, J. Garcia-Torres, C. Aleman, *ACS Biomater. Sci. Eng.* **2020**, 6, 6228.
- [101] Y. Lee, H. Kim, Y. Kim, S. Noh, B. Chun, J. Kim, C. Park, M. Choi, K. Park, J. Lee, J. Seo, *Nanoscale* **2021**, 13, 18112.
- [102] M. Y. Shen, S. Yuran, Y. Aviv, H. Ayalew, C. H. Luo, Y. H. Tsai, M. Reches, H. H. Yu, R. Shenhar, *ACS Appl. Mater. Interfaces* **2019**, 11, 1201.
- [103] M. Zhu, Y. Hao, X. Ma, L. Feng, Y. X. Zhai, Y. P. Ding, G. S. Cheng, *RSC Adv.* **2019**, 9, 12667.
- [104] N. Paradee, J. Thanokiang, A. Sirivat, *Mater. Sci. Eng. C* **2021**, 118, 111346.
- [105] H. L. Hou, L. Cardo, D. Mancino, B. Arnaiz, A. Criado, M. Prato, *Nanoscale* **2020**, 12, 23824.
- [106] X. Peng, K. Dong, Y. F. Zhang, L. L. Wang, C. H. Wei, T. M. Lv, Z. L. Wang, Z. Wu, *Adv. Funct. Mater.* **2022**, 32, 2112241.
- [107] J. W. Zhong, Y. Zhang, Q. Z. Zhong, Q. Y. Hu, B. Hu, Z. L. Wang, J. Zhou, *ACS Nano* **2014**, 8, 6273.
- [108] Q. Zheng, H. Zhang, B. J. Shi, X. Xue, Z. Liu, Y. M. Jin, Y. Ma, Y. Zou, X. X. Wang, Z. An, W. Tang, W. Zhang, F. Yang, Y. Liu, X. L. Lang, Z. Y. Xu, Z. Li, Z. L. Wang, *ACS Nano* **2016**, 10, 6510.
- [109] Z. Liu, Y. Ma, H. Ouyang, B. J. Shi, N. Li, D. J. Jiang, F. Xie, D. Qu, Y. Zou, Y. Huang, H. Li, C. C. Zhao, P. C. Tan, M. Yu, Y. Fan, H. Zhang, Z. L. Wang, Z. Li, *Adv. Funct. Mater.* **2019**, 29, 1807560.

- [110] H. Ryu, H. M. Park, M. K. Kim, B. Kim, H. S. Myoung, T. Y. Kim, H. J. Yoon, S. S. Kwak, J. Kim, T. H. Hwang, E. K. Choi, S. W. Kim, *Nat. Commun.* **2021**, *12*, 4374.
- [111] a) S. Du, H. N. Suo, G. Xie, Q. Q. Lyu, M. Mo, Z. J. Xie, N. Y. Zhou, L. B. Zhang, J. Tao, J. T. Zhu, *Nano Energy* **2022**, *93*, 106906; b) G. Yao, D. W. Jiang, J. Li, L. Kang, S. H. Chen, Y. Long, Y. Z. Wang, P. Huang, Y. Lin, W. Cai, X. Wang, *ACS Nano* **2019**, *13*, 12345; c) Y. Long, H. Wei, J. Li, G. Yao, B. Yu, D. L. Ni, A. L. F. Gibson, X. L. Lan, Y. D. Jiang, W. B. Cai, X. D. Wang, *ACS Nano* **2018**, *12*, 12533; d) L. M. Zhao, Z. B. Gao, W. Liu, C. L. Wang, D. Luo, S. Y. Chao, S. W. Li, Z. Li, C. Wang, J. Zhou, *Nano Energy* **2022**, *103*, 107798.
- [112] a) S. C. Yao, X. Y. Zhao, X. Y. Wang, T. Huang, Y. M. Ding, J. M. Zhang, Z. Y. Zhang, Z. L. Wang, L. L. Li, *Adv. Mater.* **2022**, *34*, 2109568; b) S. C. Yao, M. J. Zheng, Z. Wang, Y. C. Zhao, S. B. Wang, Z. R. Liu, Z. Li, Y. Q. Guan, Z. L. Wang, L. L. Li, *Adv. Mater.* **2022**, *34*, 2205881; c) B. B. Chu, X. Qin, Q. Q. Zhu, H. Y. Wang, Z. Wen, X. H. Sun, Y. He, S. T. Lee, *Nano Energy* **2022**, *100*, 107471; d) H. M. Li, C. Y. Chen, Z. C. Wang, Y. M. Huang, G. Q. He, Y. Liu, P. Jiang, Z. L. Wang, *Mater. Today* **2023**, *64*, 40.
- [113] Z. R. Liu, J. H. Nie, B. Miao, J. D. Li, Y. B. Cui, S. Wang, X. D. Zhang, G. R. Zhao, Y. B. Deng, Y. H. Wu, Z. Li, L. L. Li, Z. L. Wang, *Adv. Mater.* **2019**, *31*, 1807795.
- [114] a) I. M. Imani, B. Kim, X. Xiao, N. Rubab, B. J. Park, Y. J. Kim, P. Zhao, M. K. Kang, S. W. Kim, *Adv. Sci.* **2023**, *10*, 2204801; b) R. Shi, J. S. Zhang, J. J. Tian, C. C. Zhao, Z. Li, Y. Z. Zhang, Y. S. Li, C. G. Wu, W. Tian, Z. Li, *Nano Energy* **2020**, *77*, 105201.
- [115] Z. R. Liu, X. Liang, H. H. Liu, Z. Wang, T. Jiang, Y. Y. Cheng, M. Q. Wu, D. L. Xiang, Z. Li, Z. L. Wang, L. L. Li, *ACS Nano* **2020**, *14*, 15458.
- [116] Q. L. Ouyang, X. L. Feng, S. Y. Kuang, N. Panwar, P. Y. Song, C. B. Yang, G. Yang, X. Y. Hemu, G. Zhang, H. S. Yoon, J. P. Tam, B. Liedberg, G. Zhu, K. T. Yong, Z. L. Wang, *Nano Energy* **2019**, *62*, 610.
- [117] C. S. Wu, P. Jiang, W. Li, H. Y. Guo, J. Wang, J. Chen, M. R. Prausnitz, Z. L. Wang, *Adv. Funct. Mater.* **2020**, *30*, 1907378.
- [118] C. Y. Wang, G. Q. He, H. H. Zhao, Y. Lu, P. Jiang, W. Li, *Adv. Mater.* **2023**, <https://doi.org/10.1002/adma.202311246>.
- [119] P. Y. Song, S. S. Kuang, N. Panwar, G. Yang, D. J. H. Tng, S. C. Tjin, W. J. Ng, M. B. A. Majid, G. Zhu, K. T. Yong, Z. L. Wang, *Adv. Mater.* **2017**, *29*, 1605668.
- [120] T. L. Wang, H. Ouyang, Y. P. Luo, J. T. Xue, E. G. Wang, L. Zhang, Z. F. Zhou, Z. Q. Liu, X. F. Li, S. Tan, Y. X. Chen, L. P. Nan, W. T. Cao, Z. Li, F. Chen, L. P. Zheng, *Sci. Adv.* **2024**, *10*, eadi6799.
- [121] S. K. Sailapu, C. Menon, *Adv. Sci.* **2022**, *9*, 2203690.
- [122] a) S. Dutta, R. Patil, T. Dey, *Nano Energy* **2022**, *96*, 107074; b) C. Ji, J. W. Hou, K. Wang, Y. H. Ng, V. Chen, *Angew. Chem. Int. Ed.* **2017**, *56*, 9762; c) J. L. Zhang, Y. H. Wang, K. Huang, K. J. Huang, H. Jiang, X. M. Wang, *Nano Energy* **2021**, *84*, 105853.
- [123] a) D. Pankratov, E. González-Arribas, Z. Blum, S. Shleev, *Electroanalysis* **2016**, *28*, 1250; b) A. J. Bandodkar, J. M. You, N. H. Kim, Y. Gu, R. Kumar, A. M. V. Mohan, J. Kurniawan, S. Imani, T. Nakagawa, B. Parish, M. Parthasarathy, P. P. Mercier, S. Xu, J. Wang, *Energy Environ. Sci.* **2017**, *10*, 1581; c) M. Cadet, S. Gounel, C. Stines-Chaumeil, X. Brilland, J. Rouhana, F. Louerat, N. Mano, *Biosens. Bioelectron.* **2016**, *83*, 60.
- [124] X. J. Wang, M. Falk, R. Ortiz, H. M. Matsumura, J. Bobacka, R. Ludwig, M. Bergelin, L. Gorton, S. Shleev, *Biosens. Bioelectron.* **2012**, *31*, 219.
- [125] J. Gineitytė, R. Meškys, M. Dagys, D. Ratautas, *J. Power Sources* **2019**, *441*, 227163.
- [126] Y. Guo, C. R. Chen, J. Y. Feng, L. Y. Wang, J. J. Wang, C. Q. Tang, X. M. Sun, H. S. Peng, *Small Methods* **2022**, *6*, 2200142.
- [127] X. X. Xiao, K. D. McGourty, E. Magner, *J. Am. Chem. Soc.* **2020**, *142*, 11602.
- [128] I. Jeerapan, J. R. Sempionatto, J. R. You, J. Wang, *Biosens. Bioelectron.* **2018**, *122*, 284.
- [129] H. Lee, Y. T. Guo, J. L. Ross, S. Schoen Jr., F. L. Degertekin, C. Arvanitis, *Sci. Adv.* **2022**, *8*, eadd2288.
- [130] H. Teymourian, F. Tehrani, K. Longardner, K. Mahato, T. Podhajny, J. M. Moon, Y. G. Kotagiri, J. R. Sempionatto, I. Litvan, J. Wang, *Nat. Rev. Neuro.* **2022**, *18*, 497.
- [131] D. A. Domingo-Lopez, G. Lattanzi, L. H. J. Schreiber, E. J. Wallace, R. Wylie, J. O'Sullivan, E. B. Dolan, G. P. Duffy, *Adv. Drug Deliv. Rev.* **2022**, *185*, 114280.
- [132] A. L. Reiss, B. Jo, L. Folland-Ross, M. Marzelli, P. Mazaika, G. Tong, H. Y. Shen, Z. T. Li, B. Buckingham, T. Aye, R. Kingman, N. H. White, A. M. Arbelaez, L. Levandoski, E. Tsalikian, M. Tansey, J. Coffey, R. Bisbee, S. A. Weinzimer, W. Tamborlane, A. Stephen, K. Weyman, N. Maura, L. A. Fox, K. Englen, K. Bird, K. Ponthieux, J. Marrero, A. Cato, J. Lum, *Nat. Commun.* **2022**, *13*, 4940.



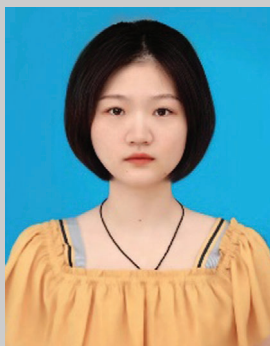
Guang-Qin He earned her bachelor's degree from Chongqing University. She is currently studying for a master's degree at School of Pharmaceutical Sciences, Wuhan University. Her current research focuses on IDDSSs.



Haimei Li received her Ph.D. degree (2023) from Wuhan University of Science and Technology. Currently, she is a postdoctor at School of Pharmaceutical Sciences, Wuhan University. Her research interests include theranostic nanomaterials, wearable devices and tumor treatment systems.



Junyi Liu received her bachelor's degree from the University of Maryland, College Park with Magna Cum Laude in Biological Sciences: Neurobiology and Physiology. She is currently a M.D. candidate at Albany Medical College in New York. Her current research focuses on cardiothoracic surgery and general surgery.



Yu-Lin Hu is currently studying for a master's degree at School of Pharmaceutical Sciences, Wuhan University. Her research interests are mainly focused on multifunctional diagnostic/therapeutic nanomaterials.



Yi Liu graduated from the Department of Chemistry at Wuhan University where, he also concluded his B. Sc., M.Sc. and Ph.D. programs. He is currently a distinguished professor at the College of Chemistry and Molecular Sciences at Wuhan University and vice president of Tiangong University. His research focuses on the synthesis, biological effect and application of nanomaterials, and multifunctional molecular probes.



Zhong Lin Wang received his Ph.D. from Arizona State University in physics. He now is the Hightower Chair in Materials Science and Engineering, Regents' Professor, Engineering Distinguished Professor, and Director, the Center for Nanostructure Characterization, at Georgia Tech. He has made original and innovative contributions to the synthesis, discovery, characterization, and understanding of fundamental physical properties of oxide nanobelts and nanowires, as well as applications of nanowires in energy sciences, electronics, optoelectronics, and biological science. He pioneered the field of piezotronics and piezo-phototronics by introducing piezoelectric potential gated charge transport process in fabricating new electronic and optoelectronic devices.



Peng Jiang received his Ph.D. degree (2013) from Wuhan University. Currently, he is an associate professor at School of Pharmaceutical Sciences, Wuhan University. He worked as a visiting scholar in Prof. Zhonglin Wang's group at Georgia Institute of Technology in 2017–2019. His research interests include fluorescent nanomaterials, theranostic nanomaterials, and self-powered functional nanodevice.